

Riemannian Covariance Fitting for Direction-of-Arrival Estimation

Joseph S. Picard, Amitay Bar, Ronen Talmon

Abstract—Covariance fitting (CF) is a comprehensive approach for direction of arrival (DoA) estimation, consolidating many common solutions. Standard practice is to use Euclidean criteria for CF, disregarding the intrinsic Hermitian positive-definite (HPD) geometry of the spatial covariance matrices. We assert that this oversight leads to inherent limitations. In this paper, as a remedy, we present a comprehensive study of the use of various Riemannian metrics of HPD matrices in CF. We focus on the advantages of the Affine-Invariant (AI) and the Log-Euclidean (LE) Riemannian metrics. Consequently, we propose a new practical beamformer based on the LE metric and derive analytically its spatial characteristics, such as the beamwidth and sidelobe attenuation, under noisy conditions. Comparing these features to classical beamformers shows significant advantage. In addition, we demonstrate, both theoretically and experimentally, the LE beamformer’s robustness in scenarios with small sample sizes and in the presence of noise, interference, and multipath channels.

Index Terms—Direction-of-arrival, beamforming, covariance fitting, Riemannian metric, MVDR and Capon’s beamformer.

I. INTRODUCTION

THE problem of direction-of-arrival (DoA) estimation has gained significant attention from the research community in recent decades, thanks to the emergence of new challenging applications. In the context of radio signals, the DoA problem consists of estimating the direction of emitters using their signals intercepted by a phased-array built of synchronized sensor elements placed at known locations. DoA estimation is long-standing and well researched [1–9], yet, it is still considered an open problem with many outstanding challenges involving high levels of noise, small sample size, multiple sources, and multipath channels. Classical DoA estimators were originally developed by invoking statistical, spectral, or spatial principles to design beamformers with some desired properties [2, 6, 10–13]. Subsequently, it has been shown that many of these classical algorithms can be recast as covariance fitting (CF) problems [14], or as variants of CF, such as signal or noise subspace fitting problems [15, 16]. Since then, CF has assumed a central role in DoA estimation both directly [7, 14, 17–19] and indirectly [13, 15, 16, 20–22]. For example, recently, CF was used as the underlying principle for improved or sparse representation of spatial spectrum [17–19], both with LASSO regularization [23] or without [20–22].

This work was supported by the European Union’s Horizon 2020 research and innovation program under grant agreement No. 802735-ERC-DIFFOP.

The authors are with the Viterbi Faculty of Electrical and Computer Engineering, Technion - Israel Institute of Technology, Haifa 32000, Israel (Corresponding author: Joseph S. Picard, email: josephp@technion.ac.il).

CF estimates the DoA by identifying the direction at which the sample covariance matrix of the intercepted signal best matches a direction-dependent model. Mathematically, it consists of fitting the sample covariance matrix $\hat{\mathbf{R}}$ to its direction-dependent model $\mathbf{R}(\theta)$, where θ is the direction¹. For example, the conventional beamformer (CB) (or delay-and-sum beamformer) for DoA estimation, which is characterized by robustness to small sample sizes, can be recast using CF by minimizing the Frobenius norm of the difference $\|\hat{\mathbf{R}} - \mathbf{R}\|_F$, or from a geometric standpoint, their Euclidean distance. Similarly, the minimum variance distortionless response (MVDR) beamformer, which is also known as the Capon beamformer and is typically characterized by a narrow mainlobe, is obtained by minimizing $\|\hat{\mathbf{R}}^{-1} - \mathbf{R}^{-1}\|_F$ (see details in Section II). The commonality between the two minimization criteria raises the question whether the Euclidean metric is necessarily the most appropriate metric for CF. Since the Euclidean distance (i.e., the Frobenius norm) between matrices equals the Euclidean distance between their vectorization and since it is computed element-wise, we argue that alternative distances that specifically take into account the structure of covariance matrices should be considered. Subsequently, we foster the search and analysis of such distances in the context of CF.

Another argument that illustrates the potential inadequacy of the Euclidean distance is the following. The HPD covariance matrices $\hat{\mathbf{R}}$ and \mathbf{R} are invertible, and since matrix inversion is a lossless manipulation that preserves the underlying information of full-rank matrices, then $\hat{\mathbf{R}}$ and \mathbf{R} embody the same information as their inverse matrices. Nevertheless, the two criteria, $\min \|\hat{\mathbf{R}} - \mathbf{R}\|_F$ and $\min \|\hat{\mathbf{R}}^{-1} - \mathbf{R}^{-1}\|_F$, yield two fundamentally different solutions (the CB and the MVDR beamformer, respectively, with an inherent tradeoff between mainlobe width and robustness to small sample sizes), while, from an information standpoint, they are similar. Furthermore, many standard signal processing procedures apply an invertible weighting matrix \mathbf{W} to the array-received signals, for example, tapering (windowing functions, e.g., Hamming, Blackman, etc.) that lowers the sidelobe levels at the expense of mainlobe broadening [1]. Indeed, $\|\hat{\mathbf{R}} - \mathbf{R}\|_F \neq \|\mathbf{W}\hat{\mathbf{R}}\mathbf{W}^H - \mathbf{W}\mathbf{R}\mathbf{W}^H\|_F$, and therefore, through CF, lead to different beamformers with an embedded tradeoff between the sidelobe level and the mainlobe width. It is therefore plausible that the two tradeoffs indicated above stem from the use of the Euclidean distance. We will show that using non-Euclidean distances between the covariance matrices mitigates these tradeoffs.

¹For brevity, we will omit the explicit dependence of \mathbf{R} on θ in the sequel.

The search for an alternative distance for CF naturally aligns with the particular geometry of covariance matrices. Indeed, the covariance matrices $\hat{\mathbf{R}}$ and \mathbf{R} are Hermitian positive definite (HPD), thereby lying on the Riemannian manifold constituted by the HPD space endowed with a Riemannian metric [24, 25]. Research involving the geometry of HPD matrices has drawn a lot of interest in recent years, introducing a plethora of new Riemannian geometries that include new metrics, geodesics, and distances, defined on the space of HPD matrices [26, 27]. These Riemannian geometries have been employed in a broad range of applications, e.g., in computer vision and medical data analysis, showing significant advantages over their Euclidean counterparts [28–32].

In this paper, we present a general framework for CF, which accommodates both Euclidean and Riemannian metrics. We utilize this framework to specify the advantages of the affine-invariant (AI) metric [24, 25, 33], which is arguably the most popular Riemannian metric, over the Euclidean metric in the context of DoA estimation problems. In addition, we study other Riemannian metrics and establish their exact relationships to classical DoA methods. Then, we focus on the log-Euclidean (LE) metric [34, 35], which approximates the AI metric on the Riemannian manifold of HPD matrices and has more efficient implementations, and propose a new beamformer induced by this LE metric. We analytically derive closed-form expressions for the spatial characteristics of the new LE beamformer, such as the beamwidth and sidelobe attenuation. We then compare these expressions with that of classical estimators in noisy conditions using new analytic expressions that account for noise, thereby revealing its advantages over classical estimators in terms of these characteristics. We theoretically and experimentally showcase the robustness of the LE beamformer in scenarios characterized by small sample size, the presence of noise and interfering sources, and multipath channels. Expanding our investigation beyond Riemannian metrics, we also examine the utilization of other non-Euclidean metrics, such as the Kullback-Liebler divergence [36], and the Log-Determinant distance [37].

It is noteworthy that in the last few years, several pioneering papers on CF using Riemannian distances rather than the classical Euclidean distance have been published. However, a comprehensive framework for the Riemannian approach has not yet been presented. Indeed, in [38], Coutino et al. introduced a new beamformer, which was inspired by Information Geometry and is tightly related to the AI metric. However, this beamformer considers only a degenerate approximation of the AI distance, and it also requires incident signals with unit power. In [39], the authors partly circumvented this overly stringent requirement by introducing a scaling parameter. In their work, the sources are not required to have unit power, but they are still required to have identical power. In [40], Chahrour et al. introduced a DoA estimator for radar signals relying on the definition of the AI distance instead of its LE approximation. However, this method holds only in the case of Toeplitz covariance matrices, and the Toeplitz property is exploited in a preliminary step for the evaluation of the reflection coefficients of incident radar signals. As a consequence, the incident power is treated as a known parameter during

the DoA estimation procedure. Another related work is [41], where the Kullback-Leibler divergence between distributions was considered as a criterion for CF in the context of DoA estimation of acoustic emitters. This has a tight connection to the present work because the AI distance between covariance matrices can be cast as a Fisher-Rao divergence between normal distributions parameterized by these matrices [42]. Extending the scope of CF, the Riemannian mean of covariance matrices has also been considered in [43], where improved robustness against interfering sources in DoA estimation was shown.

With respect to these existing works [38–40], our contribution is threefold. First, we present a geometric CF framework for DoA estimation, which provides new insights into existing methods and facilitates the development of a new class of Riemannian geometry-based methods. We exploit this framework to highlight the advantages of Riemannian metrics over the Euclidean metric. Second, we propose a new DoA estimator that relies on the LE Riemannian metric and compare it analytically to other metrics and beamformers using closed-form expressions, thereby demonstrating analytically its advantages. Third, we show that the spatial characteristics (e.g., the beamwidth and sidelobes attenuation) of the proposed LE estimator are advantageous at low signal to noise ratio (SNR) and small sample size.

The remainder of this paper is structured as follows. In Section II, we recast classical beamformers as CF problems involving the Euclidean metric, thereby defining a CF framework for DoA estimation. We highlight some limitations that stem from the Euclidean metric when used as a fitting criterion in DoA estimation problems, and we present how Riemannian metrics overcome these limitations, putting a special focus on the AI metric. In Section III, we present the LE beamformer, derived for DoA estimation, along with analytical expressions for some characteristics of the spatial spectrum. In Section IV, we show that classical non-Euclidean distances of HPD matrices systematically yield the CB and the MVDR beamformer, or variants of these two, thereby further demonstrating the novelty of the LE beamformer. In Section V, we present simulations that showcase the performance and analysis of the proposed LE beamformer.

II. COVARIANCE FITTING FRAMEWORK FOR DOA ESTIMATION

A. Notations & Acronyms

Unless stated otherwise, we use the following notation. Lowercase letters are used for scalars (e.g., s), uppercase letters for integers (e.g., K), lowercase bold letters for vectors (e.g., \mathbf{v}), and uppercase bold letters for matrices (e.g., \mathbf{M}). The conjugate, transpose, conjugate transpose, and pseudo-inverse operators are denoted by the superscripts $(\cdot)^*$, $(\cdot)^T$, $(\cdot)^H$, and $(\cdot)^\dagger$, respectively.

B. Data Model & Classical Estimators

Consider a phased-array consisting of M sensors, and let \mathbf{a}_θ denote the array's unit-norm response vector to a wave propagating from direction θ . Consider also a far-field

source transmitting a narrow-band signal from direction θ_1 . The signal collected by the phased-array at discrete time $k \in \{1, \dots, K\}$ is the complex vector $\mathbb{C}^M \ni \mathbf{y}_k = \mathbf{a}_1 x_k + \mathbf{n}_k$, where $\mathbf{a}_1 \triangleq \mathbf{a}_{\theta_1}$ is the phased-array response to the incident signal propagating from direction θ_1 , the complex scalar x_k is the k -th sample of the unknown incident signal, the vector $\mathbf{n}_k \in \mathbb{C}^M$ is a zero-mean Gaussian measurement noise with known covariance $\sigma_n^2 \mathbf{I}$, and K is the number of time samples. Without loss of generality, suppose the noise level is $\sigma_n^2 = 1$. The *sample* covariance matrix of the phased-array received signal is given by

$$\hat{\mathbf{R}} \triangleq \frac{1}{K} \sum_{k=1}^K \mathbf{y}_k \mathbf{y}_k^H, \quad (1)$$

and it commonly serves as the input of DoA estimation algorithms. The *population* covariance matrix, obtained by considering the expected value of the sample covariance matrix, is of great interest for theoretical analyses since it has an explicit expression, given by

$$\bar{\mathbf{R}} \triangleq \mathbb{E}[\hat{\mathbf{R}}] = \sigma_1^2 \mathbf{a}_1 \mathbf{a}_1^H + \mathbf{I}, \quad (2)$$

where σ_1^2 is the incident power of the source. The SNR is equal to σ_1^2 since the noise level is $\sigma_n^2 = 1$. The population covariance matrix adheres to the following model of a signal propagating from direction θ with incident power σ^2 ,

$$\mathbf{R} = \sigma^2 \mathbf{a}_\theta \mathbf{a}_\theta^H + \mathbf{I}. \quad (3)$$

The dependence of \mathbf{R} on θ and σ^2 is omitted for brevity.

Two classical DoA estimators are the CB, also referred to as Bartlett or the Delay-and-Sum beamformer [6], and the MVDR beamformer, referred to as Capon beamformer [44]. These beamformers consist of evaluating the spatial spectra $P_{\text{CB}}(\theta)$ and $P_{\text{MV}}(\theta)$ defined in their standard form by [2]

$$P_{\text{CB}}(\theta) = \mathbf{a}_\theta^H \hat{\mathbf{R}} \mathbf{a}_\theta, \quad (4)$$

$$P_{\text{MV}}(\theta) = \frac{1}{\mathbf{a}_\theta^H \hat{\mathbf{R}}^{-1} \mathbf{a}_\theta}, \quad (5)$$

where MV stands for MVDR for conciseness.

C. Direction-Finding by Covariance Fitting

The CB and MVDR beamformer have been originally derived following statistical, spatial, and spectral considerations. A different and, arguably, more intuitive approach is CF. Following algebraic considerations, it simply consists of matching the covariance matrix $\hat{\mathbf{R}}$ to its theoretical model \mathbf{R} given in (3). The goodness-of-fit criterion for two matrices \mathbf{M}_1 and \mathbf{M}_2 is usually the Frobenius norm of their element-wise difference $\mathbf{M}_1 - \mathbf{M}_2$, i.e., the Euclidean distance of their vectorizations,

$$d_E(\mathbf{M}_1, \mathbf{M}_2) \triangleq \|\mathbf{M}_1 - \mathbf{M}_2\|_F. \quad (6)$$

We show in Appendix I that the CB and MVDR beamformer consist of fitting $\hat{\mathbf{R}}$ to \mathbf{R} , and $\hat{\mathbf{R}}^{-1}$ to \mathbf{R}^{-1} , respectively,

$$P_{\text{CB}}(\theta) = \underset{\sigma^2}{\operatorname{argmin}} d_E(\hat{\mathbf{R}}, \mathbf{R}), \quad (7)$$

$$P_{\text{MV}}(\theta) = \underset{\sigma^2}{\operatorname{argmin}} d_E(\hat{\mathbf{R}}^{-1}, \mathbf{R}^{-1}). \quad (8)$$

In other words, the CB in (4) and MVDR beamformer in (5) can be recast as CF problems in (7) and (8), respectively, when the fitting criterion is the Euclidean distance.

On the one hand, using the Frobenius norm of the difference as a goodness-of-fit criterion is efficient and practical. On the other hand, this criterion operates element-wise and does not take into account that the correlation matrices are not any matrices but HPD, thereby neglecting important information.

D. Covariance Fitting based on the Affine-Invariant Metric

Here, we focus on the AI metric [24, 25]. Formally, the distance between the HPD covariance matrices $\hat{\mathbf{R}}$ and \mathbf{R} induced by the AI metric is given by [24, 45]

$$d_{\text{AI}}^2(\hat{\mathbf{R}}, \mathbf{R}) = \left\| \log(\hat{\mathbf{R}}^{-1/2} \mathbf{R} \hat{\mathbf{R}}^{-1/2}) \right\|_F^2, \quad (9)$$

$$= \sum_{m=1}^M \log^2 \left(\lambda_m \left\{ \hat{\mathbf{R}}^{-1/2} \mathbf{R} \hat{\mathbf{R}}^{-1/2} \right\} \right), \quad (10)$$

where $\lambda_m\{\cdot\}$ is the m -th largest eigenvalue of a matrix.

Then, we use the AI distance instead of the Euclidean distance in (7) and (8), and the spatial spectrum obtained by minimizing the AI distance is defined by

$$P_{\text{AI}}(\theta) = \underset{\sigma^2}{\operatorname{argmin}} \sum_{m=1}^M \log^2 \left(\lambda_m \left\{ \hat{\mathbf{R}}^{-1/2} \mathbf{R} \hat{\mathbf{R}}^{-1/2} \right\} \right). \quad (11)$$

We assert that such a distance is likely a better goodness-of-fit criterion for CF purposes in DoA estimation problems than the Euclidean distance for two reasons. First, the AI distance exploits the HPD structure of covariance matrices. Second, more specifically, minimizing each Euclidean criterion $d_E(\hat{\mathbf{R}}, \mathbf{R})$, $d_E(\hat{\mathbf{R}}^{-1}, \mathbf{R}^{-1})$, or $d_E(\mathbf{W} \hat{\mathbf{R}} \mathbf{W}^H, \mathbf{W} \mathbf{R} \mathbf{W}^H)$, where \mathbf{W} is an invertible matrix, leads to a different solution, thereby giving rise to the abovementioned tradeoffs between the sidelobe level, the mainlobe width, and the robustness to small samples. Conversely, the invariance of the AI to inversion and congruence [36] implies that $d_{\text{AI}}(\hat{\mathbf{R}}, \mathbf{R}) = d_{\text{AI}}(\hat{\mathbf{R}}^{-1}, \mathbf{R}^{-1}) = d_{\text{AI}}(\mathbf{W} \hat{\mathbf{R}} \mathbf{W}^H, \mathbf{W} \mathbf{R} \mathbf{W}^H)$, consolidating the solutions and mitigating any tradeoff between them. Indeed, we show empirically that using the AI distance as a fitting criterion leads to a beamformer with spatial spectrum with a narrow mainlobe, low sidelobes, and insensitivity to small sample sizes (see Fig. 3 in the sequel).

Importantly, we note that the problem in (11) presents a significant advantage over previous work because no assumption is made on σ^2 , and it is considered as an unknown parameter of the model covariance \mathbf{R} . Conversely, in [38–40], it was assumed that all the signals have unit power or identical power, or even that the incident power is estimated in a preliminary procedure [40, RBA Algo.]. Furthermore, the problem in (11) embodies another possible advantage compared with [38, 39], since it exploits all the eigenvalues instead of using merely the largest one. Finally, in contrast to the methods proposed in [38–40], the spatial spectrum in (11) does not suffer from scaling issues (see more details in Section IV-D).

III. THE LOG-EUCLIDEAN BEAMFORMER

Given the data model $\mathbf{R} = \sigma^2 \mathbf{a}_\theta \mathbf{a}_\theta^H + \mathbf{I}$ in (3), our assumption is that the problem in (11) has no closed-form solution. Therefore, evaluating $P_{\text{AI}}(\theta)$ requires an exhaustive search over a wide range of values of σ^2 . Performing this search for each θ requires immense computational resources, especially because the eigenvalues have to be re-evaluated for each power hypothesis σ^2 . As a remedy, we propose to consider the LE metric [34], which approximates the AI metric, and to derive a new beamformer that relies on it. In this section, we present the derivation and analysis of the beamformer based on the LE metric. The LE distance between the HPD covariance matrices $\hat{\mathbf{R}}$ and \mathbf{R} is defined by

$$d_{\text{LE}}^2(\hat{\mathbf{R}}, \mathbf{R}) = \left\| \log(\hat{\mathbf{R}}) - \log(\mathbf{R}) \right\|_F^2. \quad (12)$$

For simplicity, we use \log both as scalar logarithm and logarithm of a matrix, depending on the context. Similarly to the AI metric, the LE metric is invariant to inversion [34]. Additionally, as a tight approximation of the AI metric, the LE metric also approximately admits the invariance to congruence, but not *stricto sensu* [34].

Definition 1 (Log-Euclidean Beamformer). *The LE beamformer is defined as the minimizer of the LE distance between the covariance matrix $\hat{\mathbf{R}}$ and the model \mathbf{R} , i.e.,*

$$P_{\text{LE}}(\theta) = \underset{\sigma^2}{\operatorname{argmin}} d_{\text{LE}}^2(\hat{\mathbf{R}}, \mathbf{R}). \quad (13)$$

Proposition 1 (Explicit expression of the LE beamformer). *If the model is $\mathbf{R} = \sigma^2 \mathbf{a}_\theta \mathbf{a}_\theta^H + \mathbf{I}$ as in (3), then the LE spatial spectrum has a closed-form expression given by*

$$P_{\text{LE}}(\theta) = \exp\left(\mathbf{a}_\theta^H \log(\hat{\mathbf{R}}) \mathbf{a}_\theta\right) - 1. \quad (14)$$

The proof appears in Appendix II-A.

In the remainder of this section, we present the spatial characteristics of the LE beamformer and provide closed-form expressions for the fadings and sidelobes directions, the half-power beamwidth (HPBW), the peak-to-sidelobe ratio (PSLR), and the sensitivity to multipath. In addition, we demonstrate the advantages of the LE spectrum over the CB and MVDR spectra in terms of these characteristics. To this end, for analysis purposes, we consider the population covariance matrix $\hat{\mathbf{R}} = \sigma_1^2 \mathbf{a}_1 \mathbf{a}_1^H + \mathbf{I}$ defined in (2) instead of the sample covariance matrix $\hat{\mathbf{R}}$ defined in (1). In this case, the spatial spectrum $P_{\text{LE}}(\theta)$ reduces to (see Appendix II-B)

$$P_{\text{LE}}(\theta) = (\sigma_1^2 + 1)^{b_\theta} - 1, \quad (15)$$

where b_θ denotes the beampattern [1] or array factor [3], defined as the response of the phased-array in direction θ to an incident wave propagating from an arbitrary direction θ_1 ,

$$b_\theta \triangleq \left| \mathbf{a}_\theta^H \mathbf{a}_1 \right|^2. \quad (16)$$

Equation (15) indicates that the spectrum $P_{\text{LE}}(\theta)$ depends on θ through b_θ exclusively. Similarly, one can check that this observation also applies to the spectra $P_{\text{MV}}(\theta)$ and $P_{\text{CB}}(\theta)$ evaluated using the population covariance matrix, thereby revealing that the variable of interest is actually b_θ . Therefore,

we propose to characterize and compare the LE, MVDR and CB beamformers through the lens of the beampattern b_θ instead of θ . We will demonstrate that considering b_θ also offers the advantage of yielding SNR-dependent characteristics (further details by the end of this section), which contribute to highlight the advantages of the LE beamformer at low SNR.

Proposition 2 (Fadings and sidelobes of the LE beamformer). *Since the LE spectrum in (15) monotonically increases with b_θ , then the fadings and the sidelobes of $P_{\text{LE}}(\theta)$ occur at the same directions as those of the beampattern b_θ .*

As an example, for a uniform linear array (ULA) with M elements separated by d_λ wavelengths, the beampattern takes the following form of a Dirichlet-like kernel [2],

$$b_\theta = \frac{\sin^2(M\pi d_\lambda (\cos\theta - \cos\theta_1))}{M^2 \sin^2(\pi d_\lambda (\cos\theta - \cos\theta_1))}. \quad (17)$$

The fading and sidelobe directions of the beampattern b_θ are described by closed-form expressions obtained by identifying its local minima and maxima [2]. Based on these expressions, it follows from Proposition 2 that the fading and sidelobe directions of the LE spectrum are

$$\theta \approx \arccos(\cos\theta_1 \pm (\ell + \zeta)/(Md_\lambda)) \quad \text{for } \ell = 1, 2, \dots, \quad (18)$$

where $\zeta = 0$ for fadings and $\zeta = \frac{1}{2}$ for sidelobes.

Back to the general case for further characterization of the proposed LE beamformer, denote by θ_1 the mainlobe direction of an arbitrary spatial spectrum $P(\theta)$, and by θ_{BW} the direction at which the mainlobe drops to half of its peak value, i.e., θ_{BW} satisfies $P(\theta_{\text{BW}}) = \frac{1}{2}P(\theta_1)$.

Definition 2 (Half-power beamwidth of a spatial spectrum). *The half-power beamwidth (HPBW) of a spatial spectrum $P(\theta)$ is defined as the angular separation*

$$\text{HPBW} \triangleq |\theta_{\text{BW}} - \theta_1|. \quad (19)$$

Existing closed-form expressions for the HPBW have been derived for classical beamformers in the *absence* of noise and are therefore independent of the SNR [1–4]. For example, it has been reported in [1] that in the case of ULAs, the HPBW is $\frac{0.89}{(M-1)d_\lambda}$, which is indeed independent of the SNR. HPBW expressions reported in [1–4] actually hold only in the *absence* of noise, which is unrealistic in practice. In contrast, we are interested in a HPBW expression that depends on the SNR in order to better illustrate the advantages of the LE beamformer in the *presence* of noise. Since the definition of θ_{BW} relies on $P(\theta)$, which itself depends on the SNR, then θ_{BW} also depends on the SNR, and so does $b_{\text{BW}} \triangleq b_{\theta_{\text{BW}}}$, defined as the beampattern evaluated in direction θ_{SL} . Thus, to consider the dependence on the SNR, we recast the HPBW as a function of b_{BW} .

Proposition 3 (Half-power beamwidth as a function of b_{BW}). *The first-order approximation of the HPBW defined in (19) is*

$$\text{HPBW} = \frac{1}{\|\hat{\mathbf{a}}_1\|} \sqrt{1 - b_{\text{BW}}}, \quad (20)$$

where $\hat{\mathbf{a}}_1$ denotes the derivative of \mathbf{a}_θ with respect to θ .

TABLE I
SPATIAL PROPERTIES OF THE LOG-EUCLIDEAN, THE CONVENTIONAL AND THE MVDR BEAMFORMERS

Beamformer	Spectrum (15)	Mainlobe beamwidth (21)	Peak-to-sidelobe ratio (23)	Power under-estimation due to multipath (25)
Log-Euclidean $P_{LE}(\theta)$	$(\sigma_1^2 + 1)^{b_\theta} - 1$	$\frac{1}{\ \hat{\mathbf{a}}_1\ } \sqrt{1 - \frac{\log(\sigma_1^2/2 + 1)}{\log(\sigma_1^2 + 1)}}$	$\frac{\sigma_1^2}{(\sigma_1^2 + 1)^{b_{SL}} - 1}$	$(\sigma_1^2 + \sigma_2^2 + 1)^{\frac{1}{1 + \sigma_2^2/\sigma_1^2}} - 1$
Conventional $P_{CB}(\theta)$	$(b_\theta \sigma_1^2 + 1)$	$\frac{1}{\ \hat{\mathbf{a}}_1\ } \sqrt{\frac{1}{2} + \frac{1}{2} \frac{1}{\sigma_1^2}}$	$\frac{\sigma_1^2 + 1}{b_{SL} \sigma_1^2 + 1}$	$(\sigma_1^2 + 1)$
MVDR $P_{MV}(\theta)$	$\frac{(\sigma_1^2 + 1)}{\sigma_1^2(1 - b_\theta) + 1}$	$\frac{1}{\ \hat{\mathbf{a}}_1\ } \sqrt{\frac{1}{\sigma_1^2}}$	$(1 - b_{SL}) \sigma_1^2 + 1$	$\frac{(\sigma_1^2 + \sigma_2^2 + 1)}{(\sigma_2^2 + 1)}$

The proof appears in Appendix II-C. We now specialize (20) to the case of the LE beamformer presented in this paper.

Proposition 4 (Half-power beamwidth of the LE beamformer). *In the case of the LE beamformer in (15), the HPBW defined in (20) has the following closed-form expression,*

$$HPBW_{LE} = \frac{1}{\|\hat{\mathbf{a}}_1\|} \sqrt{1 - \frac{\log(\sigma_1^2/2 + 1)}{\log(\sigma_1^2 + 1)}}. \quad (21)$$

Proof. Equation (15) yields that $P_{LE}(\theta_{BW}) = (\sigma_1^2 + 1)^{b_{BW}} - 1$. Furthermore, we have $P_{LE}(\theta_{BW}) = P_{LE}(\theta_1)/2$ by definition. By combining these two expressions for $P_{LE}(\theta_{BW})$ and recalling that $P_{LE}(\theta_1) = \sigma_1^2$, we get after a few manipulations that $b_{BW} = \frac{\log(\sigma_1^2/2 + 1)}{\log(\sigma_1^2 + 1)}$. Substituting this result in (20) yields the HPBW expression in (21). \square

The expression for b_{BW} obtained in the above proof depends exclusively on σ_1^2 , thereby on the SNR. In turn, the HPBW of the LE beamformer, established in (21), also depends on the SNR. Note that as the SNR increases, the HPBW decreases.

Definition 3 (Peak-to-sidelobe ratio of a spatial spectrum). *The peak-to-sidelobe ratio (PSLR) of a spatial spectrum $P(\theta)$ is defined as the following power spectrum ratio*

$$PSLR \triangleq \frac{P(\theta_1)}{P(\theta_{SL})}, \quad (22)$$

where θ_{SL} denotes the direction of the closest sidelobe.

The PSLR in (22) is usually evaluated for classical beamformers in the *absence* of noise [1–4]. For example, the reported PSLR in the case of ULAs is about 13.26 [dB], which is clearly independent on the SNR. Conversely, in order to exhibit the advantages of the LE beamformer, we propose to evaluate the PSLR in (22) in the *presence* of noise, by using a population covariance matrix that accounts for noise.

Proposition 5 (Peak-to-sidelobe ratio of the LE beamformer). *In the case of the LE beamformer in (15), the PSLR defined in (22) has the following closed-form expression,*

$$PSLR_{LE} \triangleq \frac{P_{LE}(\theta_1)}{P_{LE}(\theta_{SL})} = \frac{\sigma_1^2}{(\sigma_1^2 + 1)^{b_{SL}} - 1}, \quad (23)$$

where b_{SL} is the beam pattern evaluated in direction θ_{SL} .

Proof. According to (15), we have $P_{LE}(\theta_1) = (\sigma_1^2 + 1)^{b_1} - 1$ where b_1 denotes the beam pattern b_θ evaluated in direction θ_1 .

Eq. (16) yields that $b_1 = 1$, thus $P_{LE}(\theta_1) = \sigma_1^2$. Furthermore, it also follows from (15) that $P_{LE}(\theta_{SL}) = (\sigma_1^2 + 1)^{b_{SL}} - 1$. Substituting these expressions in (22) directly yields (23). \square

In order to compare the LE beamformer with the CB and MVDR beamformer, we also evaluate the spectra $P_{CB}(\theta)$ and $P_{MV}(\theta)$ using the population covariance matrix. Then, using (20) and (22), we obtain HPBW and PSLR expressions for the CB and MVDR beamformer. The resulting expressions for the power spectra, the HPBW and the PSLR are reported in Table I. As observed in the case of the LE beamformer, these expressions for the CB and MVDR beamformer all depend on θ through b_θ .

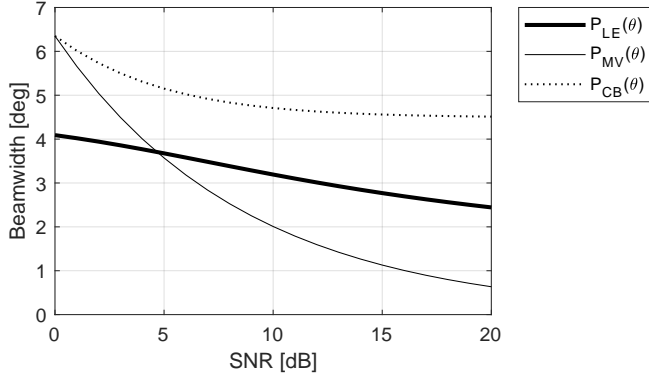
The HPBW of the LE, CB and MVDR spectra are presented in Fig. 1a in the case of a ULA with $M = 10$ elements and a source in the boresight direction $\theta_1 = 90$ [deg] for SNR values ranging from 0 to 20 [dB]. The HPBW of the LE spectrum is plotted in Fig. 1a (thick line) together with those of the MVDR spectrum (thin line) and the CB spectrum (dotted line). Fig. 1a indicates that for SNR lower than 5 [dB], the thinnest mainlobe is that of the LE spectrum. The PSLR of the LE, CB and MVDR spectra are presented in Fig. 1b. It appears that the best PSLR is clearly that of the LE spectrum (thick line), towards which the MVDR spectrum (thin line) asymptotically tends to, while that of the CB spectrum (dotted line) converges to the 13.26 [dB] level reported in [1–4]. Fig. 1 demonstrates the advantages of the LE beamformer over its Euclidean counterparts, namely the CB and the MVDR beamformer, especially at low SNR, in terms of PSLR and HPBW.

Consider now a two-ray multipath channel. Besides the signal-of-interest (SoI) in direction θ_1 with incident power σ_1^2 , a fully coherent signal in direction θ_2 with incident power σ_2^2 impinges on the phased array, thereby corrupting the DoA estimates of the SoI. Denote by ρ the complex scalar with unit magnitude that models the phase difference between the two coherent rays. Then, the population covariance matrix is

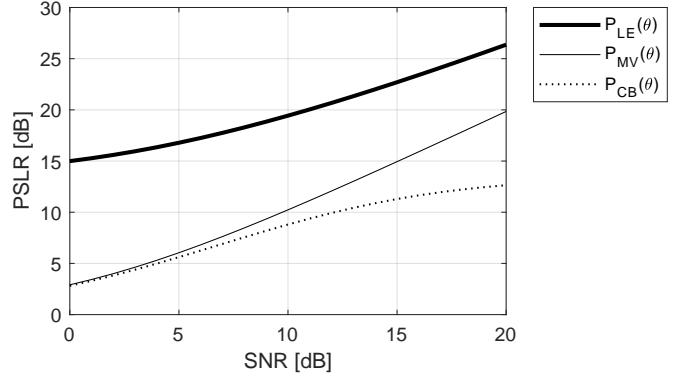
$$\bar{\mathbf{R}}_2 = (\sigma_1 \mathbf{a}_1 + \rho \sigma_2 \mathbf{a}_2)(\sigma_1 \mathbf{a}_1 + \rho \sigma_2 \mathbf{a}_2)^H + \mathbf{I}. \quad (24)$$

Denote by $P_{LE}(\theta|\bar{\mathbf{R}}_2)$, $P_{MV}(\theta|\bar{\mathbf{R}}_2)$ and $P_{CB}(\theta|\bar{\mathbf{R}}_2)$ the LE, MVDR and CB spectra evaluated in the presence of multipath using $\bar{\mathbf{R}}_2$, instead of \mathbf{R} that ignores multipath.

Proposition 6 (SoI power estimates in multipath conditions). *Suppose that θ_1 and θ_2 are sufficiently separated such that θ_2*



(a) Half-power beamwidth (HPBW).



(b) Peak-to-sidelobe ratio (PSLR).

Fig. 1. Half-power beamwidth (HPBW) and peak-to-sidelobe ratio (PSLR) evaluated using the population covariance matrix, for the Log-Euclidean beamformer $P_{LE}(\theta)$, the MVDR beamformer $P_{MV}(\theta)$ and the Conventional beamformer $P_{CB}(\theta)$. Case of a ULA with $M = 10$ antennas and a single source at boresight.

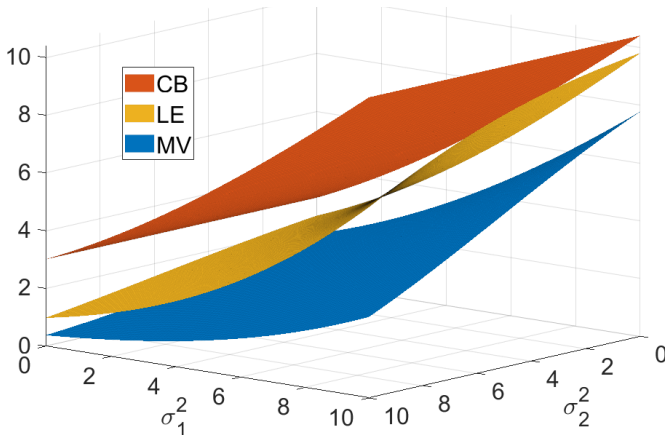


Fig. 2. The approximate power spectra $P_{CB}(\theta_1|\bar{\mathbf{R}}_2)$, $P_{LE}(\theta_1|\bar{\mathbf{R}}_2)$, and $P_{MV}(\theta_1|\bar{\mathbf{R}}_2)$ given in (25), (26) and (27), as a function of σ_1^2 and σ_2^2 .

(the direction of the multipath ray) is away from the mainlobe of the SoI propagating from direction θ_1 . Then, the power estimates in the SoI direction, obtained from the LE, MVDR, and CB spectra, are given by

$$P_{LE}(\theta_1|\bar{\mathbf{R}}_2) \approx (\sigma_1^2 + 1 + \sigma_2^2) \frac{\sigma_1^2}{\sigma_1^2 + \sigma_2^2} - 1, \quad (25)$$

$$P_{MV}(\theta_1|\bar{\mathbf{R}}_2) \approx (\sigma_1^2 + 1 + \sigma_2^2) / (\sigma_2^2 + 1), \quad (26)$$

$$P_{CB}(\theta_1|\bar{\mathbf{R}}_2) \approx (\sigma_1^2 + 1). \quad (27)$$

The proof and details on the approximation appear in Appendix III. It is noteworthy that the expressions in (25), (26) and (27) are independent of θ_1 .

Ideally, the power estimates in the SoI direction should not be affected by multipath, i.e., it should be as close as possible to σ_1^2 for the LE beamformer and to $\sigma_1^2 + 1$ for the CB and MVDR beamformer. Eq. (27) indicates that this ideal robustness is achieved by the CB. To illustrate the robustness of the LE beamformer to multipath, the expressions (25), (26) and (27) are numerically evaluated and presented in Fig. 2 for a grid of values of σ_1^2 and σ_2^2 spanning from 0 to 10 [dB]. We see in Fig. 2 that in the presence of multipath, the LE spectrum slightly under-estimates the SoI power, outperforming the MVDR spectrum, which significantly under-estimates it.

IV. ALTERNATIVE METRICS FOR COVARIANCE FITTING IN DOA ESTIMATION PROBLEMS

To complement the analysis and to enhance the difference between the proposed LE beamformer (14), which is a low-complexity approximation of the AI beamformer (11), and the CB and MVDR beamformer, we show in this section that other metrics systematically yield the CB and MVDR beamformer, or variants and combinations of which. The considered metrics and their respective spatial spectra are summarized in Table II.

A. Covariance Fitting based on the Kullback-Leibler Distance

In the Information Geometry framework, the covariance matrices \mathbf{R} and $\hat{\mathbf{R}}$ fully describe the zero-mean Gaussian distribution of the model and the samples. The Kullback-Leibler (KL) divergence is a well-known measure for the distance between two such distributions, its expression is [36]

$$d_{KL}(\hat{\mathbf{R}}, \mathbf{R}) \triangleq \text{Tr}(\mathbf{R}^{-1}\hat{\mathbf{R}} - \mathbf{I}) - \log \text{Det}(\mathbf{R}^{-1}\hat{\mathbf{R}}). \quad (28)$$

The KL divergence is not invariant to inversion and congruence. The spatial spectrum obtained by minimizing the KL distance is (see Supplementary Material, Appendix VI)

$$P_{KL}^{(1)}(\theta) \triangleq \underset{\sigma^2}{\text{argmin}} d_{KL}^2(\hat{\mathbf{R}}, \mathbf{R}) = \mathbf{a}_\theta^H \hat{\mathbf{R}} \mathbf{a}_\theta - 1, \quad (29)$$

which is similar to the spectrum of the CB beamformer (4) up to the inconsequential offset -1 . Since the KL divergence is not symmetric, we get that the spatial spectrum obtained by minimizing $d_{KL}(\mathbf{R}, \hat{\mathbf{R}})$ instead of $d_{KL}(\hat{\mathbf{R}}, \mathbf{R})$ is (see Supplementary Material, Appendix VI)

$$P_{KL}^{(2)}(\theta) \triangleq \underset{\sigma^2}{\text{argmin}} d_{KL}^2(\mathbf{R}, \hat{\mathbf{R}}) = \frac{1}{\mathbf{a}_\theta^H \hat{\mathbf{R}}^{-1} \mathbf{a}_\theta} - 1, \quad (30)$$

which coincides with the spectrum of the MVDR beamformer (5) up to a constant offset -1 .

TABLE II
BEAMFORMERS AND DOA-ESTIMATORS OBTAINED BY COVARIANCE FITTING FOR DIFFERENT METRICS

BEAMFORMER		DISTANCE MINIMIZATION	SPATIAL SPECTRUM	SHRINKAGE
Conventional	$P_{CB}(\theta)$	$\min_{\sigma^2} d_E^2(\hat{\mathbf{R}}, \mathbf{R}) = \left\ \hat{\mathbf{R}} - \mathbf{R} \right\ _F^2$	$\mathbf{a}_\theta^H \hat{\mathbf{R}} \mathbf{a}_\theta$	$g(\lambda) = \lambda$
MVDR (Capon)	$P_{MV}(\theta)$	$\min_{\sigma^2} d_E^2(\hat{\mathbf{R}}^{-1}, \mathbf{R}^{-1}) = \left\ \hat{\mathbf{R}}^{-1} - \mathbf{R}^{-1} \right\ _F^2$	$\frac{1}{\mathbf{a}_\theta^H \hat{\mathbf{R}}^{-1} \mathbf{a}_\theta}$	$g(\lambda) = -\frac{1}{\lambda}$
Log-Euclidean	$P_{LE}(\theta)$	$\min_{\sigma^2} d_{LE}^2(\hat{\mathbf{R}}, \mathbf{R}) = \left\ \log(\hat{\mathbf{R}}) - \log(\mathbf{R}) \right\ _F^2$	$\exp\left(\mathbf{a}_\theta^H \log(\hat{\mathbf{R}}) \mathbf{a}_\theta\right) - \sigma_n^2$	$g(\lambda) = \log(\lambda)$
Affine-Invariant	$P_{AI}(\theta)$	$\min_{\sigma^2} d_{AI}^2(\hat{\mathbf{R}}, \mathbf{R}) = \left\ \log(\hat{\mathbf{R}}^{-1/2} \mathbf{R} \hat{\mathbf{R}}^{-1/2}) \right\ _F^2$	NA	NA
Kullback-Leibler (1)	$P_{KL}^{(1)}(\theta)$	$\min_{\sigma^2} d_{KL}^2(\hat{\mathbf{R}}, \mathbf{R}) = \text{Tr}(\mathbf{R}^{-1} \hat{\mathbf{R}} - \mathbf{I}) - \log \text{Det}(\mathbf{R}^{-1} \hat{\mathbf{R}})$	$\mathbf{a}_\theta^H \hat{\mathbf{R}} \mathbf{a}_\theta - \sigma_n^2$	$g(\lambda) = \lambda$
Kullback-Leibler (2)	$P_{KL}^{(2)}(\theta)$	$\min_{\sigma^2} d_{KL}^2(\mathbf{R}, \hat{\mathbf{R}}) = \text{Tr}(\hat{\mathbf{R}}^{-1} \mathbf{R} - \mathbf{I}) - \log \text{Det}(\hat{\mathbf{R}}^{-1} \mathbf{R})$	$\frac{1}{\mathbf{a}_\theta^H \hat{\mathbf{R}}^{-1} \mathbf{a}_\theta} - \sigma_n^2$	$g(\lambda) = -\frac{1}{\lambda}$
Log-Determinant	$P_{LD}(\theta)$	$\min_{\sigma^2} d_{LD}^2(\hat{\mathbf{R}}, \mathbf{R}) = \log\left(\text{Det}\left\{\frac{\hat{\mathbf{R}} + \mathbf{R}}{2}\right\}\right) - \frac{1}{2} \log\left(\text{Det}\{\hat{\mathbf{R}}\mathbf{R}\}\right)$	$\frac{1}{\mathbf{a}_\theta^H (\hat{\mathbf{R}} + \sigma_n^2 \mathbf{I})^{-1} \mathbf{a}_\theta} - 2\sigma_n^2$	$g(\lambda) = -\frac{1}{\lambda + \sigma_n^2}$

B. Covariance Fitting based on the Log-Determinant Metric

The Log-Determinant (LD) distance between the HPD covariance matrices $\hat{\mathbf{R}}$ and \mathbf{R} is defined by [37]

$$d_{LD}^2(\hat{\mathbf{R}}, \mathbf{R}) \triangleq \log\left(\text{Det}\left\{\frac{\hat{\mathbf{R}} + \mathbf{R}}{2}\right\}\right) - \frac{\log(\text{Det}\{\hat{\mathbf{R}}\mathbf{R}\})}{2}. \quad (31)$$

The spatial spectrum obtained by minimizing the LD distance defined in (31) is given by (proof in Supp. Material, App. VII)

$$P_{LD}(\theta) = \frac{1}{\mathbf{a}_\theta^H (\hat{\mathbf{R}} + \mathbf{I})^{-1} \mathbf{a}_\theta} - 2, \quad (32)$$

implying that the LD beamformer is a variant of the MVDR beamformer with unit diagonal loading and correction of the power offset. Furthermore, the LD distance is invariant to matrix inversion and congruence (see Supplementary Material, Appendix VII). As mentioned in [46, p. 9], although it approximates the AI metric, the log-Determinant metric is not a Riemannian metric *stricto sensu*.

C. Relation to Shrinkage

When the sample size is small, a common technique for covariance matrix estimation is to manipulate (“shrink”) the eigenvalues of the sample covariance matrix (e.g., see [47]). Consider the decomposition of the covariance matrix $\hat{\mathbf{R}}$ into eigenvalues λ_m and unit-norm eigenvectors \mathbf{u}_m such that $\hat{\mathbf{R}} = \sum_{m=1}^M \lambda_m \mathbf{u}_m \mathbf{u}_m^H$. Then, the spectrum $P_{CB}(\theta)$ in (4), the spectrum $P_{MV}(\theta)$ in (5), and the spectrum $P_{LE}(\theta)$ in (14) can be recast as follows

$$\begin{aligned} P_{CB}(\theta) &= \sum_m |\mathbf{a}_\theta^H \mathbf{u}_m|^2 \lambda_m, \\ P_{MV}(\theta) &= \left(\sum_m |\mathbf{a}_\theta^H \mathbf{u}_m|^2 \lambda_m^{-1} \right)^{-1}, \\ P_{LE}(\theta) &= \exp\left(\sum_m |\mathbf{a}_\theta^H \mathbf{u}_m|^2 \log(\lambda_m) \right) - 1. \end{aligned} \quad (33)$$

Neglecting constant scalar offsets, these three spectra adhere to a generic spectrum model, given by

$$P(\theta) \triangleq g^{-1}\left(\sum_m |\mathbf{a}_\theta^H \mathbf{u}_m|^2 g(\lambda_m) \right), \quad (34)$$

where $g: \mathbb{R}^+ \rightarrow \mathbb{R}^+$ is a monotonically increasing function that operates on the eigenvalues of the covariance matrix. The functions $g(\cdot)$ corresponding to the considered beamformers are presented in the rightmost column of Table II².

D. Relation to Existing Riemannian Approaches

Define $d_{(M')}^2(\theta)$ from $d_{AI}^2(\theta)$ by truncating the summation in (10) to keep only the M' largest eigenvalues,

$$d_{(M')}^2(\hat{\mathbf{R}}, \mathbf{R}) = \sum_{m=1}^{M'} \log^2\left(\lambda_m \left\{ \hat{\mathbf{R}}^{-1/2} \mathbf{R} \hat{\mathbf{R}}^{-1/2} \right\}\right). \quad (35)$$

In the case of a single signal, the beamformers proposed in [38–40] can be written as

$$\begin{aligned} P_{[38]}(\theta) &= \frac{1}{d_{(1)}^2(\hat{\mathbf{R}}, \mathbf{a}_\theta \mathbf{a}_\theta^H)}, \\ P_{[39]}(\theta) &= \frac{1}{d_{(1)}^2(\eta \hat{\mathbf{R}}, \mathbf{a}_\theta \mathbf{a}_\theta^H)}, \\ P_{[40]}(\theta) &= \frac{1}{d_{(M)}^2(\hat{\mathbf{R}}, \mathbf{a}_\theta \mathbf{a}_\theta^H + \eta' \mathbf{I})}, \end{aligned} \quad (36)$$

where the scaling parameters η and η' are defined by $\eta \triangleq (\hat{\sigma}_1^2 + \hat{\sigma}_n^2/M)^{-1}$ and $\eta' \triangleq \text{std}\{\text{diag}\{\mathbf{a}_\theta \mathbf{a}_\theta^H\}\}$, and where $(\hat{\sigma}_1^2, \hat{\sigma}_n^2)$ are Maximum-Likelihood estimates for (σ_1^2, σ_n^2) .

In Section II-D, we outlined advantages of the proposed LE and AI beamformers over the beamformers presented in [38–40]. Another advantage of the AI and LE beamformers concerns the physical meaning of the spatial spectra. The AI beamformer $P_{AI}(\theta)$, the LE beamformer $P_{LE}(\theta)$, and the other beamformers in Table II as well, have spatial spectra expressed in power units, the same power units as σ_1^2 , σ_n^2 and $\hat{\mathbf{R}}$. Conversely, in (35) and (36), we see that due to the square-logarithm transformation, the units of the spatial spectra $P_{[38]}(\theta)$, $P_{[39]}(\theta)$ and $P_{[40]}(\theta)$ are not power units, but some arbitrary units devoid of physical meaning. For

²We also claim that the celebrated MUSIC and MODE beamformers are closely related to the generic model (34), but it is beyond the scope of this paper.

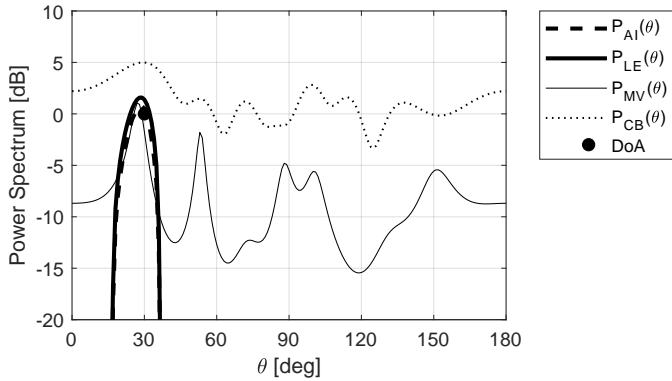


Fig. 3. The power spectra $P_{AI}(\theta)$, $P_{LE}(\theta)$, $P_{MV}(\theta)$ and $P_{CB}(\theta)$. The source direction is 30 [deg] and the incident SNR is 0 [dB] (black circle).

example, power units should not be arbitrary in order to ensure meaningful PSLR analyses. Therefore, the beamformers $P_{[38]}(\theta)$, $P_{[39]}(\theta)$ and $P_{[40]}(\theta)$ cannot be directly considered as power spectra without educated manipulations and heuristic calibrations.

V. SIMULATIONS & NUMERICAL EXAMPLES

In this section, we numerically demonstrate the properties of the proposed LE beamformer $P_{LE}(\theta)$, whose closed-form expression is given in (14), and compare it to the CB, the MVDR beamformer, and the Riemannian AI beamformer.

A. Spatial spectrum at low SNR and small sample size

In the first experiment, the considered phased-array is a ULA consisting of $M = 9$ antennas with a half-wavelength antenna separation. This ULA intercepts a signal with SNR of 0 [dB] propagating from direction 30 [deg]. The source direction is intentionally chosen away from boresight to add an extra layer of complexity because phased-arrays are less discriminative at endfire. The number of samples is $K = 10$, which only critically exceeds the number of antennas. For each sample k , the measurement noise \mathbf{n}_k is a zero-mean complex Gaussian vector of length M with covariance matrix \mathbf{I} , since the noise power is $\sigma_n^2 = 1$. The signal x_k is a zero-mean constant modulus signal with phase uniformly drawn in $[0, 2\pi]$. Figure 3 presents the spatial power spectrum for the proposed LE beamformer $P_{LE}(\theta)$ (thick line), where it is compared to the MVDR beamformer $P_{MV}(\theta)$ (thin line), the CB $P_{CB}(\theta)$ (dotted line), and to the AI spectrum $P_{AI}(\theta)$ (dashed line). The true direction of the source is depicted by a black circle. We see that the multiple peaks in the MVDR spectrum $P_{MV}(\theta)$ are misleading and erroneously indicate signals in directions where none exists, e.g., in direction 53 [deg]. The spectrum of the CB $P_{CB}(\theta)$ fluctuates around the 0 [dB] noise level, and even the actual direction is hardly identifiable. Conversely, the proposed LE power spectrum $P_{LE}(\theta)$ has a single, unambiguous lobe in the actual DoA. In addition, we see that the LE spectrum is similar to the AI spectrum but obtained much more efficiently through a closed-form expression rather than based on an exhaustive, computationally demanding search.

In the second experiment, the ULA is composed of $M = 16$ antennas and four uncorrelated signals propagating from directions 30 [deg], 60 [deg], 90 [deg] and 120 [deg]. The SNRs of the incident signals are 5 [dB], 4 [dB], 3 [dB] and 0 [dB], respectively. The number of samples is $K = 20$. Figure 4a compares the spatial power spectrum for the proposed LE beamformer $P_{LE}(\theta)$ (thick line) with that of the MVDR beamformer and the CB (thin and dotted lines, respectively). We see here as well that the LE spectrum $P_{LE}(\theta)$ exhibits unambiguous and clearly identifiable lobes at the sources directions (black circles). Conversely, the peaks in the MVDR and CB spectra are less distinct, and there are peaks in directions where no source exists, e.g., in direction 140 [deg].

An even more challenging scenario is considered in Figure 4b, in which three of the four signals are fully coherent (marked by black circles), e.g., representing the case of a line-of-sight ray degraded by two multipath rays. Only the fourth signal is kept uncorrelated (marked by a white circle). The phase differences between the line-of-sight ray and the two multipath rays, implemented as phasors, are arbitrarily set to $-\frac{2\pi}{3}$ and $+\frac{\pi}{2}$. We see in the figure that the LE spectrum identifies all the DoAs. Conversely, besides the strongest coherent signal at direction 30, the MVDR (thin line) fails to identify all the other DoAs, including the uncorrelated one. The CB (dotted line) exhibits in the actual DoAs some small lobes emerging above the noise-level fluctuations, but these lobes are clearly inferior to the lobes obtained by the proposed LE beamformer (thick line). However, the “sharpness” of the LE peaks is obtained at the expense of under-estimation of the signal power for each DoA.

We repeat the experiment presented in Fig. 4a, with four uncorrelated signals with decreasing powers and DoAs separated by 30 [deg], 200 times using i.i.d. realizations of the signals and noise, leading to different sample covariance matrices. The phased-array remains unchanged with $M = 16$ elements and the number of samples is set to $K = 20$, scarcely more than the number of antennas. The resulting spatial spectra are presented in Fig. 5, where the shades indicate the 5 and 95 percentiles for each of the beamformers. We see that the LE beamformer consists of sharp thin lobes at the directions of the signals, in contrast to the spatial spectra obtained by the other beamformers.

In the third experiment, we consider a dominant signal in direction $\theta_1 = 30$ [deg] and an uncorrelated weak signal in direction $\theta_2 = 60$ [deg]. The dominant signal SNR is increased from -10 to 50 [dB] while maintaining the weak signal power at 15 [dB] below the dominant signal power. The DoAs of the dominant and weak signals are estimated as the directions of the two largest peaks in the spatial power spectrum. The obtained RMSE for 200 realizations with respect to the dominant signal as a function of the dominant signal SNR is presented in Fig. 6a. For reference, we also present the Cramér-Rao bound (CRB). We see that for a dominant signal SNR from -10 [dB] to 30 [dB], the estimation errors of the dominant signal direction θ_1 obtained by the CB and the LE beamformer are similar and slightly better than that of the MVDR beamformer. Beyond 30 [dB], the estimation error obtained by the CB beamformer increases because of

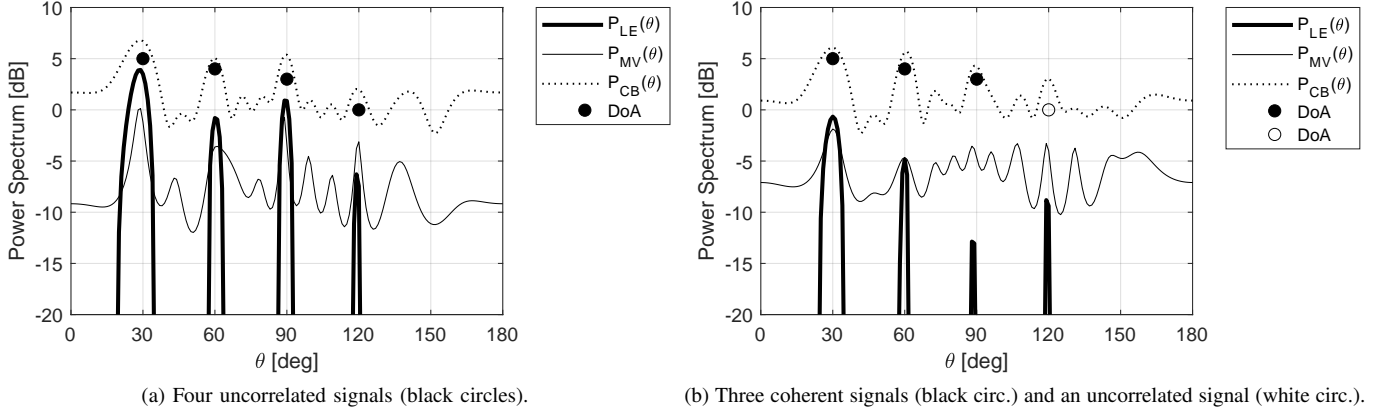


Fig. 4. Power spectra of the proposed LE beamformer $P_{LE}(\theta)$, the MVDR beamformer $P_{MV}(\theta)$, and the CB $P_{CB}(\theta)$. Four signals propagate from directions 30 [deg], 60 [deg], 90 [deg], and 120 [deg] with respective SNRs: 5 [dB], 4 [dB], 3 [dB], and 0 [dB].

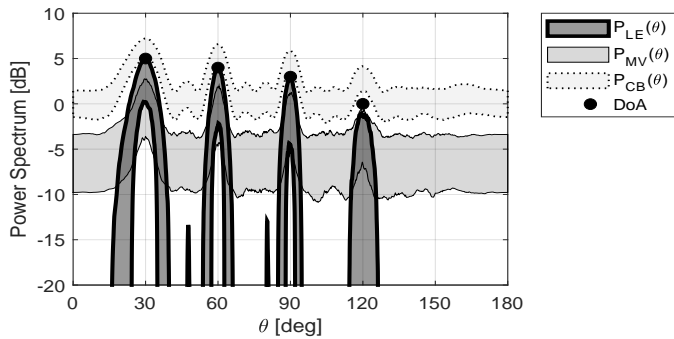


Fig. 5. Sleeves of the 5 and 95 percentiles of the Log-Euclidean, the MVDR and the Conventional beamformers.

the mainlobe bias induced by the weak signal. Conversely, the LE and MVDR errors are low, with a clear advantage for the MVDR beamformer at extremely high SNR. In addition, we see that for SNR values from 10 [dB] to 30 [dB], the LE estimator is optimal as it meets the CRB with respect to θ_1 . Note that in (unrealistic) high SNR values, the MVDR also meets the bound.

In Fig. 6b, we present the root-mean-square error (RMSE) of the weak signal DoA estimates as a function of the weak signal SNR based on 200 realizations. Here, we see that the LE beamformer outperforms both the CB and the MVDR beamformer. The MVDR beamformer behaves poorly because the small sample size makes the sample covariance poorly conditioned, and its inverse is then degraded by large errors. The CB performs even worse because the second largest peak in the CB spectrum is erroneously interpreted as the weak signal direction, but it is in fact one of the dominant signal sidelobes whose directions are 46 [deg] and 162 [deg] according to (18). The resulting RMSE of the CB is then $\sqrt{((46 - \theta_2)^2 + (162 - \theta_2)^2)/2} \approx 72$ [deg]. This result is in accordance with the RMSE of the CB in Fig. 6b. Conversely, the LE beamformer neither requires inverting the covariance matrix nor suffers from high sidelobes. This experiment demonstrates the advantage of the LE beamformer in recovering DoAs of weak signals. Furthermore, we see that the LE estimation of the weak signal direction is close to optimal as it almost reaches the CRB.

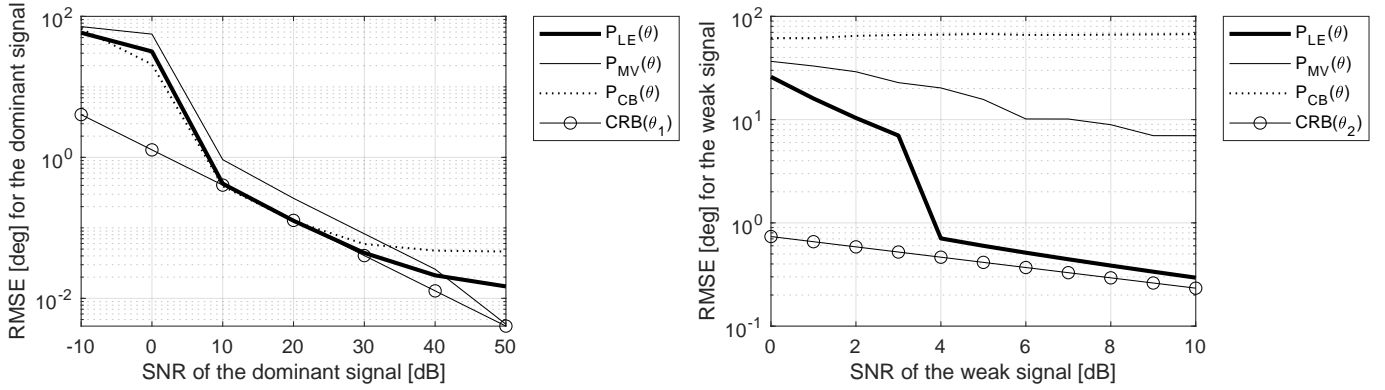
B. Demonstrating the spatial properties of the LE beamformer

We experimentally demonstrate the closed-form expressions of the spatial properties presented in Section III. The experimental setup includes a phased-array with $M = 16$ antennas, and the noise level is set to $\sigma_n^2 = 1$. Two coherent signals propagate from directions $\theta_1 = 90$ [deg] and $\theta_2 = 60$ [deg], and a third signal, uncorrelated with the other two signals, propagates from direction $\theta_3 = 30$ [deg]. The SNRs of these signals are $\sigma_1^2 = 5$ [dB], $\sigma_2^2 = 3$ [dB] and $\sigma_3^2 = 0$ [dB], respectively. The phase difference between the two coherent signals is $+\frac{\pi}{2}$. The spatial spectra of the CB, LE and MVDR beamformers, obtained using the population covariance matrix, are represented in Fig. 7a. If the multipath ray were absent, the LE power spectrum in direction θ_1 would be $\sigma_1^2 = 5$ [dB]. However, the expression in (25) predicts in the presence of the multipath ray, the power spectrum in direction θ_1 is 3.112 [dB]. Indeed, the obtained power $P_{LE}(\theta_1)$ is 3.114 [dB].

To evaluate the predicted beamwidth and sidelobe levels, the last experiment is repeated while keeping only the first signal in direction θ_1 , and removing the two other signals. The obtained spatial power spectrum is presented in Fig. 7b, focusing on the directions near $\theta_1 = 90$ [deg]. The mainlobe beamwidth predicted in (21) is 2.9 [deg], while the obtained empirical beamwidth (marked by a horizontal arrow) is 2.5 [deg]. In addition, the sidelobe level predicted in (23) is -16.78 [dB], while the obtained empirical sidelobe (marked by a vertical arrow) is -16.45 [deg]. We also see in the figure that the CB has significantly higher sidelobes, because of noise. However, even in ideal noise-free conditions, the sidelobe level is approximately -13.26 [dB] (see [2]). Therefore, despite the presence of noise, the LE sidelobe level still outperforms the ideal sidelobes of the CB.

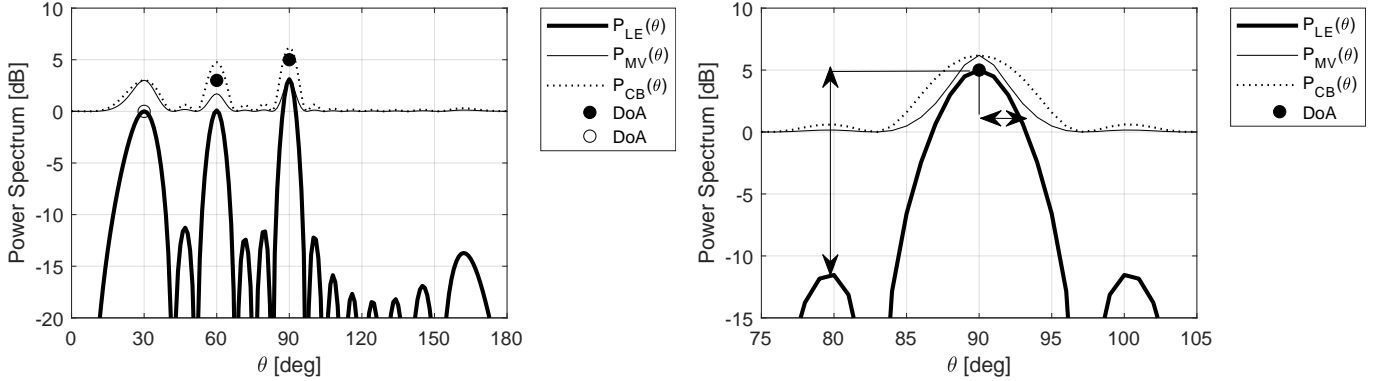
VI. CONCLUSIONS

We introduced a new beamforming approach for DoA estimation problems based on CF that offers the advantage of exploiting the HPD Riemannian geometry of the spatial covariance matrices. Following this approach, we presented a new beamformer that relies on the LE metric. This LE beamformer has a closed-form expression, enabling efficient



(a) RMSE of DoA estimates for the dominant signal as a function of its SNR. (b) RMSE of DoA estimates for the weak signal as a function of its SNR.

Fig. 6. Root-mean-square error (RMSE) of the directions estimates of the dominant and weak signals, for the LE, MVDR and Conventional beamformers (thick line, thin line and dotted line). The SNR of the two signals increase jointly while keeping their power ratio constant and equal to 15[dB].



(a) Two coherent signals (black circ.) and an uncorrelated signal (white circ.). (b) A single signal in direction $\theta_1 = 90$ [deg]. Zoom on the mainlobe.

Fig. 7. Power spectrum of the LE beamformer $P_{LE}(\theta)$, the MVDR beamformer $P_{MV}(\theta)$ and the Conventional beamformer $P_{CB}(\theta)$. The power spectra are evaluated using the population covariance matrix.

implementation and analysis of its spatial properties, demonstrating its theoretical advantages over the CB and the MVDR beamformer at low SNR. Numerical experiments illustrate additional advantages of the proposed LE beamformer over the CB and the MVDR beamformer in scenarios that include small sample size with multiple, possibly coherent, signals. These results establish that in the context of DoA estimation via CF, the LE metric, which accounts for the HPD geometry of spatial covariance matrices, is a better goodness-of-fit criterion than the Euclidean metric. In future work, we plan to incorporate common techniques of robustification such as diagonal loading in the proposed LE beamformer. The development of robust variants of the LE beamformer will allow us to extend the experimental study and to compare our results to recently-proposed beamformers for DoA estimation.

APPENDIX I COVARIANCE FITTING ACCOUNTING FOR NOISE

The spectrum $P(\theta)$ obtained by CF between $\hat{\mathbf{R}}$ and \mathbf{R} is

$$P(\theta) = \underset{\sigma^2}{\operatorname{argmin}} d_E(\hat{\mathbf{R}}, \mathbf{R}) = \operatorname{Tr} \left\{ \left((\hat{\mathbf{R}} - \mathbf{I}) - \sigma^2 \mathbf{a}_\theta \mathbf{a}_\theta^H \right)^2 \right\}. \quad (37)$$

Provided that the signal power σ^2 is not null, the value of σ^2 that minimizes the latter expression is obtained by matching to 0 the derivative w.r.t σ^2 ,

$$2\sigma^2 - 2\mathbf{a}_\theta^H (\hat{\mathbf{R}} - \mathbf{I}) \mathbf{a}_\theta = 0. \quad (38)$$

Rearranging the terms, we get (4) by setting $P(\theta) = \sigma^2$.

Consider now the spectrum $P(\theta)$ obtained by CF between $\hat{\mathbf{R}}^{-1}$ and \mathbf{R}^{-1} . Note that $\mathbf{R}^{-1} = -\alpha \mathbf{a}_\theta \mathbf{a}_\theta^H + \mathbf{I}$ where $\alpha \triangleq \frac{\sigma^2}{\sigma^2 + 1}$. We have

$$\begin{aligned} P(\theta) &= \underset{\sigma^2}{\operatorname{argmin}} d_E(\hat{\mathbf{R}}^{-1}, \mathbf{R}^{-1}) = \operatorname{Tr} \left\{ \left((\hat{\mathbf{R}}^{-1} - \mathbf{I}) + \alpha \mathbf{a}_\theta \mathbf{a}_\theta^H \right)^2 \right\} \\ &= \underset{\sigma^2}{\operatorname{argmin}} \alpha^2 + 2\alpha \mathbf{a}_\theta^H (\hat{\mathbf{R}}^{-1} - \mathbf{I}) \mathbf{a}_\theta. \end{aligned} \quad (39)$$

Provided that the signal power σ^2 is not null, the value of σ^2 that minimizes the latter expression is obtained by matching to 0 the derivative w.r.t σ^2 ,

$$\left(2\alpha + 2\mathbf{a}_\theta^H (\hat{\mathbf{R}}^{-1} - \mathbf{I}) \mathbf{a}_\theta \right) \frac{\partial \alpha}{\partial \sigma^2} = 0. \quad (40)$$

Note that $\frac{\partial \alpha}{\partial \sigma^2} = \frac{1}{(\sigma^2 + 1)^2}$. Inserting the expression for α , rearranging the latter equation, and setting $P(\theta) = \sigma^2$ yields

$$P(\theta) = \frac{1}{\mathbf{a}_\theta^H \hat{\mathbf{R}}^{-1} \mathbf{a}_\theta} - 1. \quad (41)$$

The latter expression is equivalent to the MVDR beamformer (5). This concludes the proof for our claim in Section II-C.

APPENDIX II ANALYSIS OF THE LOG-EUCLIDEAN BEAMFORMER

A. Spatial Spectrum using the Sample Covariance Matrix

The LE power spectrum $P_{LE}(\theta)$ defined in (14) consists in minimizing w.r.t. σ^2 the LE distance between $\hat{\mathbf{R}}$ and \mathbf{R} ,

$$d_{LE}^2(\hat{\mathbf{R}}, \mathbf{R}) = \left\| \log \hat{\mathbf{R}} - \log \mathbf{R} \right\|_F^2 \quad (42)$$

$$= \text{Tr} \left\{ (\log \hat{\mathbf{R}})^2 - 2 \log \hat{\mathbf{R}} \log \mathbf{R} + (\log \mathbf{R})^2 \right\}$$

The value of σ^2 that minimizes the latter expression is obtained by matching to 0 the derivative w.r.t σ^2 . We have

$$\frac{\partial d_{LE}}{\partial \sigma^2}(\hat{\mathbf{R}}, \mathbf{R}) = \text{Tr} \left\{ -2 \log \hat{\mathbf{R}} \frac{\partial \log \mathbf{R}}{\partial \sigma^2} + 2 \frac{\partial \log \mathbf{R}}{\partial \sigma^2} \log \mathbf{R} \right\}.$$

Matching the latter expression to 0 gives

$$\text{Tr} \left\{ \log \hat{\mathbf{R}} \frac{\partial \log \mathbf{R}}{\partial \sigma^2} \right\} = \text{Tr} \left\{ \frac{\partial \log \mathbf{R}}{\partial \sigma^2} \log \mathbf{R} \right\}. \quad (43)$$

Note that the eigen-decomposition of the covariance model $\mathbf{R} = \sigma^2 \mathbf{a}_\theta \mathbf{a}_\theta^H + \mathbf{I}$ takes the form

$$\mathbf{R} = [\mathbf{a}_\theta \quad \mathbf{U}_n] \begin{bmatrix} \sigma^2 + 1 & \mathbf{0} \\ \mathbf{0} & \mathbf{I} \end{bmatrix} \begin{bmatrix} \mathbf{a}_\theta^H \\ \mathbf{U}_n^H \end{bmatrix}. \quad (44)$$

where \mathbf{U}_n denotes the eigenvectors associated with the noise subspace. The matrix-logarithm of \mathbf{R} is then

$$\log \mathbf{R} = [\mathbf{a}_\theta, \mathbf{U}_n] \begin{bmatrix} \log(\sigma^2 + 1) & \mathbf{0} \\ \mathbf{0} & \mathbf{0} \end{bmatrix} \begin{bmatrix} \mathbf{a}_\theta^H \\ \mathbf{U}_n^H \end{bmatrix} = \log(\sigma^2 + 1) \mathbf{a}_\theta \mathbf{a}_\theta^H.$$

The derivative of $\log \mathbf{R}$ with respect to σ^2 is therefore $\frac{\mathbf{a}_\theta \mathbf{a}_\theta^H}{\sigma^2 + 1}$. Inserting this result in (43) gives immediately

$$\text{Tr} \left\{ \log \hat{\mathbf{R}} \frac{\mathbf{a}_\theta \mathbf{a}_\theta^H}{\sigma^2 + \sigma_n^2} \right\} = \text{Tr} \left\{ \frac{\mathbf{a}_\theta \mathbf{a}_\theta^H}{\sigma^2 + \sigma_n^2} \log \mathbf{R} \right\}. \quad (45)$$

Rearranging the terms, we get

$$\mathbf{a}_\theta^H \log(\hat{\mathbf{R}}) \mathbf{a}_\theta = \mathbf{a}_\theta^H \log(\mathbf{R}) \mathbf{a}_\theta. \quad (46)$$

Since \mathbf{a}_θ is the eigenvector of \mathbf{R} associated with the eigenvalue $\log(\sigma^2 + 1)$, then $\log(\mathbf{R}) \mathbf{a}_\theta = \log(\sigma^2 + 1) \mathbf{a}_\theta$. As a result,

$$\mathbf{a}_\theta^H \log(\hat{\mathbf{R}}) \mathbf{a}_\theta = \mathbf{a}_\theta^H (\log(\sigma^2 + 1) \mathbf{a}_\theta) = \log(\sigma^2 + 1). \quad (47)$$

Applying the exponential function on both sides gives

$$\exp \left(\mathbf{a}_\theta^H \log(\hat{\mathbf{R}}) \mathbf{a}_\theta \right) = \sigma^2 + 1. \quad (48)$$

Rearranging the latter equation and setting $P_{LE}(\theta) = \sigma^2$, we get the LE beamformer

$$P_{LE}(\theta) = \exp \left(\mathbf{a}_\theta^H \log(\hat{\mathbf{R}}) \mathbf{a}_\theta \right) - 1. \quad (49)$$

B. Spatial Spectrum using the Population Covariance Matrix

Consider the population covariance matrix $\bar{\mathbf{R}}$ given in (2) and its eigen-decomposition,

$$\bar{\mathbf{R}} = [\mathbf{a}_1, \mathbf{U}'_n] \begin{bmatrix} \sigma_1^2 + 1 & \mathbf{0} \\ \mathbf{0} & \mathbf{I} \end{bmatrix} \begin{bmatrix} \mathbf{a}_1^H \\ \mathbf{U}'_n{}^H \end{bmatrix}. \quad (50)$$

where \mathbf{U}'_n is the matrix of the noise-subspace eigenvectors. The matrix-logarithm of $\bar{\mathbf{R}}$ is then

$$\log \bar{\mathbf{R}} = [\mathbf{a}_1, \mathbf{U}'_n] \begin{bmatrix} \log(\sigma_1^2 + 1) & \mathbf{0} \\ \mathbf{0} & \mathbf{0} \end{bmatrix} \begin{bmatrix} \mathbf{a}_1^H \\ \mathbf{U}'_n{}^H \end{bmatrix} = \log(\sigma_1^2 + 1) \mathbf{a}_1 \mathbf{a}_1^H.$$

We now evaluate the operand in (49),

$$\mathbf{a}_\theta^H \log(\bar{\mathbf{R}}) \mathbf{a}_\theta = \log(\sigma_1^2 + 1) |\mathbf{a}_\theta^H \mathbf{a}_1|^2 = \log(\sigma_1^2 + 1) b_\theta. \quad (51)$$

where the beampattern $b_\theta \triangleq |\mathbf{a}_\theta^H \mathbf{a}_1|^2$ is introduced in (16). Inserting (51) in (49) gives

$$P_{LE}(\theta) = \exp(\log(\sigma_1^2 + 1) b_\theta) - 1 = (\sigma_1^2 + 1)^{b_\theta} - 1. \quad (52)$$

C. Derivation of the Half-Power Beamwidth (HPBW)

Consider the second-order Taylor approximation of the beampattern $b_\theta \triangleq |\mathbf{a}_1^H \mathbf{a}_\theta|^2$ in the vicinity of θ_1 ,

$$b_\theta \approx b_1 + \dot{b}_1(\theta - \theta_1) + \ddot{b}_1(\theta - \theta_1)^2/2, \quad (53)$$

where b_1 , \dot{b}_1 and \ddot{b}_1 denote the beampattern and its derivatives with respect to θ , evaluated at θ_1 . One can easily check that

$$\dot{b}_1 = \frac{\partial |\mathbf{a}_1^H \mathbf{a}_\theta|^2}{\partial \theta} \Big|_{\theta_1} = 2 \text{Re} \{ \mathbf{a}_1^H \dot{\mathbf{a}}_1 \}, \quad (54)$$

$$\ddot{b}_1 = \frac{\partial^2 |\mathbf{a}_1^H \mathbf{a}_\theta|^2}{\partial \theta^2} \Big|_{\theta_1} = 2 \text{Re} \{ \mathbf{a}_1^H \ddot{\mathbf{a}}_1 \} + 2 |\mathbf{a}_1^H \dot{\mathbf{a}}_1|^2. \quad (55)$$

Provided that the unit-norm steering vector \mathbf{a}_θ has been properly normalized, the three following identities hold:

$$\mathbf{a}_\theta^H \mathbf{a}_\theta = 1, \quad \dot{\mathbf{a}}_\theta^H \mathbf{a}_\theta = 0, \quad \ddot{\mathbf{a}}_\theta^H \mathbf{a}_\theta = - \|\dot{\mathbf{a}}_\theta\|^2, \quad (56)$$

where $\dot{\mathbf{a}}_\theta$ and $\ddot{\mathbf{a}}_\theta$ denote the derivatives of \mathbf{a}_θ with respect to θ . These three identities evaluated at θ_1 respectively yield

$$b_1 \triangleq |\mathbf{a}_1^H \mathbf{a}_1|^2 = 1, \quad \dot{b}_1 = 0, \quad \ddot{b}_1 = -2 \|\dot{\mathbf{a}}_1\|^2. \quad (57)$$

Inserting these results in (53) gives $b_\theta \approx 1 - (\theta - \theta_1)^2 \|\dot{\mathbf{a}}_1\|^2$. Rearranging the terms, we get $|\theta - \theta_1| \approx \sqrt{1 - b_\theta} / \|\dot{\mathbf{a}}_1\|$. The latter result, evaluated at $\theta = \theta_{BW}$, achieves the proof of (20).

Note that in the case of a ULA with a large number of elements, when the SNR $\sigma_1 \rightarrow \infty$, the expression (20) approaches the classical expressions for HPBW, e.g. $\frac{0.89}{M d_\lambda}$. Indeed, since $\|\dot{\mathbf{a}}_\theta\|^2 = \frac{1}{12} (2\pi d_\lambda)^2 (M^2 - 1)$ at boresight, then the *two-sided* HPBW of the CB spectrum given in Table I satisfies

$$HPBW = \frac{2}{\|\dot{\mathbf{a}}_1\|} \sqrt{\frac{1}{2} + \frac{1}{2\sigma_1^2}} \rightarrow \frac{0.78}{M d_\lambda} \approx \frac{0.89}{M d_\lambda} \quad (58)$$

APPENDIX III

POWER UNDER-ESTIMATION DUE TO MULTIPATH

A. Log-Euclidean Beamformer: Proof for (25)

Assume that the multipath in direction θ_2 is not within the beampattern of the mainlobe centered on θ_1 . Then $\mathbf{a}_1^H \mathbf{a}_2$ has a small magnitude, and the eigen-decomposition of the population matrix $\bar{\mathbf{R}}_2$ given in (24) in the case of two correlated rays takes the form

$$\bar{\mathbf{R}}_2 \approx [\mathbf{u}_s \quad \mathbf{U}_n'] \begin{bmatrix} \sigma_1^2 + \sigma_2^2 + 1 & \mathbf{0} \\ \mathbf{0} & \mathbf{I} \end{bmatrix} [\mathbf{u}_s \quad \mathbf{U}_n']^H, \quad (59)$$

where the eigenvector \mathbf{u}_s satisfies $\mathbf{u}_s = \frac{\sigma_1 \mathbf{a}_1 + \rho \sigma_2 \mathbf{a}_2}{\|\sigma_1 \mathbf{a}_1 + \rho \sigma_2 \mathbf{a}_2\|}$. Then, the matrix-logarithm of $\bar{\mathbf{R}}_2$ is $\log \bar{\mathbf{R}}_2 = \log(\sigma_1^2 + \sigma_2^2 + 1) \mathbf{u}_s \mathbf{u}_s^H$. Since $\mathbf{a}_1^H \mathbf{a}_2$ has a small magnitude, then

$$\mathbf{a}_1^H \log \bar{\mathbf{R}}_2 \mathbf{a}_1 = \log(\sigma_1^2 + \sigma_2^2 + 1) |\mathbf{a}_1^H \mathbf{u}_s|^2, \quad (60)$$

$$\approx \log(\sigma_1^2 + \sigma_2^2 + 1) \frac{\sigma_1^2}{\sigma_1^2 + \sigma_2^2}. \quad (61)$$

Then, the power spectrum in direction θ_1 is

$$P_{LE}(\theta_1 | \bar{\mathbf{R}}_2) = \exp(\mathbf{a}_1^H \log(\bar{\mathbf{R}}_2) \mathbf{a}_1) - 1, \quad (62)$$

$$= (\sigma_1^2 + \sigma_2^2 + 1) \frac{\sigma_1^2}{\sigma_1^2 + \sigma_2^2} - 1. \quad (63)$$

which concludes the proof of the expression in (25).

B. MVDR Beamformer: Proof for (26)

Consider the population covariance matrix $\bar{\mathbf{R}}_2$ in the case of two coherent signals given in (24).

$$\bar{\mathbf{R}}_2 = (\sigma_1 \mathbf{a}_1 + \rho \sigma_2 \mathbf{a}_2)(\sigma_1 \mathbf{a}_1 + \rho \sigma_2 \mathbf{a}_2)^H + \mathbf{I}. \quad (64)$$

The Searle identity [48] yields a closed-form expression for the inverse of $\bar{\mathbf{R}}_2$,

$$\bar{\mathbf{R}}_2^{-1} = -\frac{(\sigma_1 \mathbf{a}_1 + \rho \sigma_2 \mathbf{a}_2)(\sigma_1 \mathbf{a}_1 + \rho \sigma_2 \mathbf{a}_2)^H}{1 + \|\sigma_1 \mathbf{a}_1 + \rho \sigma_2 \mathbf{a}_2\|^2} + \mathbf{I}. \quad (65)$$

Left- and right-multiplying by \mathbf{a}_1 gives

$$\mathbf{a}_1^H \bar{\mathbf{R}}_2^{-1} \mathbf{a}_1 = -\frac{|\sigma_1 + \rho \sigma_2 \mathbf{a}_1^H \mathbf{a}_2|^2}{1 + \|\sigma_1 \mathbf{a}_1 + \rho \sigma_2 \mathbf{a}_2\|^2} + 1. \quad (66)$$

Since $|\mathbf{a}_1^H \mathbf{a}_2| \ll 1$, then

$$\mathbf{a}_1^H \bar{\mathbf{R}}_2^{-1} \mathbf{a}_1 \approx -\frac{\sigma_1^2}{1 + \sigma_1^2 + \sigma_2^2} + 1 = \frac{1 + \sigma_2^2}{1 + \sigma_1^2 + \sigma_2^2}. \quad (67)$$

The inverse of the left-hand side expression is identified as the MVDR spectrum in direction θ_1 . Therefore,

$$P_{MV}(\theta_1 | \bar{\mathbf{R}}_2) \approx \frac{1 + \sigma_1^2 + \sigma_2^2}{1 + \sigma_2^2}. \quad (68)$$

C. Conventional Beamformer: Proof for (27)

Consider the population covariance matrix $\bar{\mathbf{R}}_2$ in the case of two coherent signals given in (24). Then, the power spectrum in direction θ_1 , given by $P_{CB}(\theta_1 | \bar{\mathbf{R}}_2) = \mathbf{a}_1^H \bar{\mathbf{R}}_2^{-1} \mathbf{a}_1$, satisfies

$$\begin{aligned} P_{CB}(\theta_1 | \bar{\mathbf{R}}_2) &= \mathbf{a}_1^H (\sigma_1 \mathbf{a}_1 + \rho \sigma_2 \mathbf{a}_2)(\sigma_1 \mathbf{a}_1 + \rho \sigma_2 \mathbf{a}_2)^H \mathbf{a}_1 + 1 \\ &= \sigma_1^2 + 2 \operatorname{Re} \{ \mathbf{a}_1^H \mathbf{a}_2 \sigma_1 \sigma_2 \rho \} + |\mathbf{a}_1^H \mathbf{a}_2|^2 \sigma_2^2 + 1. \end{aligned}$$

Assume that the multipath in direction θ_2 is not within the beampattern of the mainlobe centered on θ_1 . Then $\mathbf{a}_1^H \mathbf{a}_2$ has a small magnitude, and we get $P_{CB}(\theta_1 | \bar{\mathbf{R}}_2) \approx \sigma_1^2 + 1$.

REFERENCES

- [1] H. Van Trees, "Optimum array processing: Part iv," in *Detection, Estimation, and Modulation Theory*. John Wiley & Sons, 2004.
- [2] P. Stoica and R. L. Moses, *Spectral analysis of signals*. Pearson Prentice Hall, NJ, 2005, vol. 452.
- [3] C. Balanis, *Antenna Theory: Analysis and Design*. Wiley, 2015.
- [4] R. Mailloux, *Phased Array Antenna Handbook*. Artech House, 2018.
- [5] M. Wax, "Model-based processing in sensor arrays," in *Advances in Spectrum Analysis and Array Processing (Vol. III)*, S. Haykin, Ed. Prentice-Hall, 1995, p. 1–47.
- [6] H. Krim and M. Viberg, "Two decades of array signal processing research: the parametric approach," *IEEE signal processing mag.*, vol. 13, no. 4, pp. 67–94, 1996.
- [7] M. Pesavento, M. Trinh-Hoang, and M. Viberg, "Three more decades in array signal processing research: An optimization and structure exploitation perspective," *IEEE Signal Processing Mag.*, vol. 40, no. 4, pp. 92–106, 2023.
- [8] S. Chakrabarty and E. A. Habets, "Broadband doa estimation using convolutional neural networks trained with noise signals," in *2017 IEEE Workshop on Applications of Signal Processing to Audio and Acoustics (WASPAA)*. IEEE, 2017, pp. 136–140.
- [9] —, "Multi-speaker doa estimation using deep convolutional networks trained with noise signals," *IEEE Journal of Selected Topics in Signal Processing*, vol. 13, no. 1, pp. 8–21, 2019.
- [10] J. Li, P. Stoica, and Z. Wang, "On robust capon beamforming and diagonal loading," *IEEE transactions on signal processing*, vol. 51, no. 7, pp. 1702–1715, 2003.
- [11] R. O. Schmidt, *A signal subspace approach to multiple emitter location and spectral estimation*. Stanford, 1982.
- [12] A. J. Weiss, B. Friedlander, and P. Stoica, "Direction-of-arrival estimation using mode with interpolated arrays," *IEEE transactions on signal processing*, vol. 43, no. 1, pp. 296–300, 1995.
- [13] M. Viberg, B. Ottersten, and T. Kailath, "Detection and estimation in sensor arrays using weighted subspace fitting," *IEEE transactions on Signal Processing*, vol. 39, no. 11, pp. 2436–2449, 1991.
- [14] B. Ottersten, P. Stoica, and R. Roy, "Covariance matching estimation techniques for array signal processing applications," *Digital Signal Processing*, vol. 8, no. 3, pp. 185–210, 1998.
- [15] B. Ottersten, M. Viberg, and T. Kailath, "Analysis of subspace fitting and ml techniques for parameter estimation from sensor array data," *IEEE Transactions on Signal Processing*, vol. 40, no. 3, pp. 590–600, 1992.
- [16] M. Wax and A. Adler, "Vector set classification by signal subspace matching," *IEEE Transactions on Information Theory*, vol. 69, no. 3, pp. 1853–1865, 2022.
- [17] M. Trinh-Hoang, M. Viberg, and M. Pesavento, "An improved doa estimator based on partial relaxation approach," in *International Conf. on Acoustics, Speech and Signal Proc. (ICASSP)*. IEEE, 2018, pp. 3246–3250.

- [18] D. Schenck, M. Trinh, H. X. Mestre, M. Viberg, and M. Pesavento, "Full covariance fitting doa estimation using partial relaxation framework," in *27th European Signal Proc. Conf. (EUSIPCO)*. IEEE, 2019, pp. 1–5.
- [19] T. Yardibi, J. Li, P. Stoica, and L. N. Cattafesta III, "Sparsity constrained deconvolution approaches for acoustic source mapping," *The Journal of the Acoustical Society of America*, vol. 123, no. 5, pp. 2631–2642, 2008.
- [20] J. S. Picard and A. J. Weiss, "Direction finding of multiple emitters by spatial sparsity and linear programming," in *9th International Symposium on Communications and Information Technology*. IEEE, 2009, pp. 1258–1262.
- [21] J. Zheng, M. Kaveh, and H. Tsuji, "Sparse spectral fitting for direction of arrival and power estimation," in *2009 IEEE/SP 15th Workshop on Statistical Signal Processing*. IEEE, 2009, pp. 429–432.
- [22] A. Delmer, A. Ferréol, and P. Larzabal, "On regularization parameter for l0-sparse covariance fitting based doa estimation," in *International Conf. on Acoustics, Speech and Signal Proc. (ICASSP)*. IEEE, 2020, pp. 4552–4556.
- [23] R. Tibshirani, "Regression shrinkage and selection via the lasso," *Journal of the Royal Statistical Society Series B: Stat. Methodology*, vol. 58, no. 1, pp. 267–288, 1996.
- [24] X. Pennec, P. Fillard, and N. Ayache, "A riemannian framework for tensor computing," *International Journal of computer vision*, vol. 66, no. 1, pp. 41–66, 2006.
- [25] R. Bhatia, *Positive definite matrices*. Princeton university press, 2009.
- [26] Y. Thanwerdas and X. Pennec, "Bures-wasserstein minimizing geodesics between covariance matrices of different ranks," *arXiv preprint arXiv:2204.09928*, 2022.
- [27] A. Han, B. Mishra, P. Jawanpuria, and J. Gao, "Generalized bures-wasserstein geometry for positive definite matrices," *arXiv preprint arXiv:2110.10464*, 2021.
- [28] A. Barachant, S. Bonnet, M. Congedo, and C. Jutten, "Multiclass brain-computer interface classification by riemannian geometry," *IEEE Transactions on Biomedical Engineering*, vol. 59, no. 4, pp. 920–928, 2011.
- [29] —, "Classification of covariance matrices using a Riemannian-based kernel for BCI applications," *Neurocomputing*, vol. 112, pp. 172–178, 2013.
- [30] P. Rodrigues, F. Bouchard, M. Congedo, and C. Jutten, "Dimensionality reduction for BCI classification using Riemannian geometry," in *BCI 2017-7th International Brain-Computer Interface Conference*, 2017.
- [31] P. L. C. Rodrigues, C. Jutten, and M. Congedo, "Riemannian procrustes analysis: transfer learning for brain-computer interfaces," *IEEE Transactions on Biomedical Engineering*, vol. 66, no. 8, pp. 2390–2401, 2018.
- [32] O. Yair, M. Ben-Chen, and R. Talmon, "Parallel transport on the cone manifold of spd matrices for domain adaptation," *IEEE Transactions on Signal Processing*, vol. 67, no. 7, pp. 1797–1811, 2019.
- [33] Y. Thanwerdas and X. Pennec, "Is affine-invariance well defined on spd matrices? a principled continuum of metrics," in *International Conference on Geometric Science of Information*. Springer, 2019, pp. 502–510.
- [34] V. Arsigny, P. Fillard, X. Pennec, and N. Ayache, "Log-euclidean metrics for fast and simple calculus on diffusion tensors," *Magnetic Resonance in Medicine: An Official Journal of the Int. Society for Magnetic Resonance in Medicine*, vol. 56, no. 2, pp. 411–421, 2006.
- [35] —, "Geometric means in a novel vector space structure on symmetric positive-definite matrices," *SIAM journal on matrix analysis and applications*, vol. 29, no. 1, pp. 328–347, 2007.
- [36] S. Chevallier, E. K. Kalunga, Q. Barthélemy, and E. Monacelli, "Review of riemannian distances and divergences, applied to ssvp-based bci," *Neuroinformatics*, vol. 19, no. 1, pp. 93–106, 2021.
- [37] S. Sra, "A new metric on the manifold of kernel matrices with application to matrix geometric means," in *Advances in neural info. proc. systems*, vol. 25, 2012, pp. 144–152.
- [38] M. Coutino, R. Pribic, and G. Leus, "Direction of arrival estimation based on information geometry," in *IEEE Intern. Conference on Acoustics, Speech and Signal Processing (ICASSP)*. IEEE, 2016, pp. 3066–3070.
- [39] Y.-Y. Dong, C.-X. Dong, W. Liu, M.-M. Liu, and Z.-Z. Tang, "Scaling transform based information geometry method for doa estimation," *IEEE Transactions on Aerospace and Electronic Systems*, vol. 55, no. 6, pp. 3640–3650, 2019.
- [40] H. Chahrour, R. Dansereau, S. Rajan, and B. Balaji, "Direction of arrival estimation using riemannian mean and distance," in *2019 IEEE Radar Conference (RadarConf)*. IEEE, 2019, pp. 1–5.
- [41] A. Weiss, "Blind direction-of-arrival estimation in acoustic vector-sensor arrays via tensor decomposition and kullback-leibler divergence covariance fitting," *IEEE Tran. on Signal Processing*, vol. 69, pp. 531–545, 2020.
- [42] J. Pinele, J. E. Strapasson, and S. I. Costa, "The fisher-rao distance between multivariate normal distributions: Special cases, bounds and applications," *Entropy*, vol. 22, no. 4, p. 404, 2020.
- [43] A. Bar and R. Talmon, "On interference-rejection using riemannian geometry for direction of arrival estimation," *arXiv preprint arXiv:2301.03399*, 2023.
- [44] J. Capon, "High-resolution frequency-wavenumber spectrum analysis," *Proceedings of the IEEE*, vol. 57, no. 8, pp. 1408–1418, 1969.
- [45] R. Bhatia and J. Holbrook, "Riemannian geometry and matrix geometric means," *Linear algebra and its applications*, vol. 413, no. 2-3, pp. 594–618, 2006.
- [46] I. Horev, F. Yger, and M. Sugiyama, "Geometry-aware principal component analysis for symmetric positive definite matrices," in *Asian Conference on Machine Learning*. PMLR, 2016, pp. 1–16.
- [47] C. Stein, "Lectures on the theory of estimation of many parameters," *Journal of Soviet Mathematics*, vol. 34, pp. 1373–1403, 1986.
- [48] D. S. Bernstein, *Matrix mathematics: theory, facts, and formulas*. Princeton university press, 2009.

SUPPLEMENTARY MATERIAL

APPENDIX IV ANALYSIS OF THE CB BEAMFORMER

A. Fadings and Sidelobes of the Spatial Spectrum

Consider the Conventional Beamformer $P_{CB}(\theta) = \mathbf{a}_\theta^H \bar{\mathbf{R}} \mathbf{a}_\theta$. According to (2), the population covariance matrix in the case of a single emitter is $\bar{\mathbf{R}} = \sigma_1^2 \mathbf{a}_1 \mathbf{a}_1^H + \mathbf{I}$, therefore

$$P_{CB}(\theta) = \mathbf{a}_\theta^H (\sigma_1^2 \mathbf{a}_1 \mathbf{a}_1^H + \mathbf{I}) \mathbf{a}_\theta \quad (69)$$

$$= \sigma_1^2 \mathbf{a}_\theta^H \mathbf{a}_1 \mathbf{a}_1^H \mathbf{a}_\theta + 1 \quad (70)$$

$$= \sigma_1^2 b_\theta + 1, \quad (71)$$

where $b_\theta \triangleq |\mathbf{a}_\theta^H \mathbf{a}_1|^2$ is the beampattern introduced in (16). Since the spectrum is a linear function of b_θ , the fadings and the sidelobes of $P_{CB}(\theta)$ occur at the same directions than the fadings and the sidelobes of the beampattern b_θ .

B. Derivation of the Beamwidth

According to (71), the CB spectrum in the actual direction θ_1 and the half-power direction θ_{BW} are

$$P_{CB}(\theta_{BW}) = \sigma_1^2 b_{BW} + 1, \quad (72)$$

$$P_{CB}(\theta_1) = \sigma_1^2 + 1. \quad (73)$$

By definition, we have $P_{CB}(\theta_{BW}) = \frac{1}{2} P_{CB}(\theta_1)$. Therefore, $\sigma_1^2 b_{BW} + 1 = \frac{1}{2} (\sigma_1^2 + 1)$. Rearranging the terms, we get

$$b_{BW} = \frac{1}{2} \left(1 - \frac{1}{\sigma_1^2} \right). \quad (74)$$

Inserting this result in the expression for BW in (20) gives

$$BW \approx \frac{1}{\|\hat{\mathbf{a}}_1\|} \sqrt{1 - b_{BW}} = \frac{1}{\|\hat{\mathbf{a}}_1\|} \sqrt{\frac{1}{2} + \frac{1}{2\sigma_1^2}}. \quad (75)$$

C. Derivation of the PSLR

The CB spectrum values in the actual direction θ_1 and the sidelobe direction θ_{SL} are:

$$P_{CB}(\theta_1) = \sigma_1^2 |\mathbf{a}_1^H \mathbf{a}_1|^2 + 1 = \sigma_1^2 + 1, \quad (76)$$

$$P_{CB}(\theta_{SL}) = \sigma_1^2 |\mathbf{a}_1^H \mathbf{a}_{SL}|^2 + 1 = \sigma_1^2 b_{SL} + 1. \quad (77)$$

where $b_{SL} \triangleq |\mathbf{a}_1^H \mathbf{a}_{SL}|^2$. Therefore, the PSLR is

$$PSLR_{CB} \triangleq \frac{P_{CB}(\theta_1)}{P_{CB}(\theta_{SL})} = \frac{\sigma_1^2 + 1}{\sigma_1^2 b_{SL} + 1}. \quad (78)$$

APPENDIX V ANALYSIS OF THE MV BEAMFORMER

A. Fadings and Sidelobes of the Spatial Spectrum

Consider the MVDR beamformer $P_{MV}(\theta) = \frac{1}{\mathbf{a}_\theta^H \bar{\mathbf{R}}^{-1} \mathbf{a}_\theta}$. Note that the inverse of the population covariance matrix $\bar{\mathbf{R}} = \sigma_1^2 \mathbf{a}_1 \mathbf{a}_1^H + \mathbf{I}$ is given by $\bar{\mathbf{R}}^{-1} = -\frac{\sigma_1^2}{\sigma_1^2 + 1} \mathbf{a}_1 \mathbf{a}_1^H + \mathbf{I}$. Then,

$$P_{MV}(\theta) = \frac{1}{\mathbf{a}_\theta^H \left(-\frac{\sigma_1^2}{\sigma_1^2 + 1} \mathbf{a}_1 \mathbf{a}_1^H + \mathbf{I} \right) \mathbf{a}_\theta} \quad (79)$$

$$= \frac{1}{-\frac{\sigma_1^2}{\sigma_1^2 + 1} b_\theta + 1} = \frac{\sigma_1^2 + 1}{\sigma_1^2 (1 - b_\theta) + 1}, \quad (80)$$

where $b_\theta \triangleq |\mathbf{a}_\theta^H \mathbf{a}_1|^2$ is introduced in (16). Since the spectrum increases with b_θ , the fadings and the sidelobes of $P_{MV}(\theta)$ occur at the same directions than the fadings and the sidelobes of the beampattern b_θ .

B. Derivation of the Beamwidth

According to (80), the MVDR spectrum in the actual direction θ_1 and the half-power direction θ_{BW} are

$$P_{MV}(\theta_{BW}) = \frac{\sigma_1^2 + 1}{\sigma_1^2 (1 - b_{BW}) + 1}, \quad (81)$$

$$P_{MV}(\theta_1) = \sigma_1^2 + 1. \quad (82)$$

By definition, we have $P_{MV}(\theta_{BW}) = \frac{1}{2} P_{MV}(\theta_1)$. Therefore,

$$\frac{\sigma_1^2 + 1}{\sigma_1^2 (1 - b_{BW}) + 1} = \frac{\sigma_1^2 + 1}{2}. \quad (83)$$

Rearranging the terms, we get $b_{BW} = 1 - \frac{1}{\sigma_1^2}$. Inserting this result in the expression for the beamwidth established in (20) gives

$$BW \approx \frac{1}{\|\hat{\mathbf{a}}_1\|} \sqrt{1 - b_{BW}} = \frac{1}{\|\hat{\mathbf{a}}_1\|} \frac{1}{\sqrt{\sigma_1^2}}. \quad (84)$$

C. Derivation of the PSLR

The MV spectrum values in the actual direction θ_1 and the sidelobe direction θ_{SL} are:

$$P_{MV}(\theta_1) = \frac{\sigma_1^2 + 1}{\sigma_1^2 (1 - |\mathbf{a}_1^H \mathbf{a}_1|^2) + 1} = \sigma_1^2 + 1, \quad (85)$$

$$P_{MV}(\theta_{SL}) = \frac{\sigma_1^2 + 1}{\sigma_1^2 (1 - b_{SL}) + 1}. \quad (86)$$

where $b_{SL} \triangleq |\mathbf{a}_1^H \mathbf{a}_{SL}|^2$. Therefore, the PSLR is

$$PSLR_{MV} \triangleq \frac{P_{MV}(\theta_1)}{P_{MV}(\theta_{SL})} = \sigma_1^2 (1 - b_{SL}) + 1. \quad (87)$$

APPENDIX VI
ANALYSIS OF THE KULLBACK-LEIBLER BEAMFORMER

Consider the model (3) for the covariance matrix. In this Appendix, we will invoke the following identities

$$\mathbf{R}^{-1}\mathbf{a}_\theta = \frac{1}{\sigma^2 + 1}\mathbf{a}_\theta, \quad (88)$$

$$\partial\mathbf{M}^{-1} = -\mathbf{M}^{-1}(\partial\mathbf{M})\mathbf{M}^{-1}, \quad (89)$$

$$\partial \log \text{Det}(\mathbf{M}) = \text{Tr} \{ \mathbf{M}^{-1}(\partial\mathbf{M}) \}. \quad (90)$$

The Kullback-Leibler (KL) power spectrum $P_{\text{KL}}^{(1)}(\theta)$ defined in (29) consists in minimizing w.r.t. σ^2 the KL divergence between $\hat{\mathbf{R}}$ and \mathbf{R} defined by

$$d_{\text{KL}}(\hat{\mathbf{R}}, \mathbf{R}) \triangleq \text{Tr} \left(\mathbf{R}^{-1}\hat{\mathbf{R}} - \mathbf{I} \right) - \log \text{Det}(\mathbf{R}^{-1}\hat{\mathbf{R}}). \quad (91)$$

The value of σ^2 that minimizes the latter expression is obtained by matching to 0 the derivative w.r.t. σ^2 . We have

$$\begin{aligned} \frac{\partial d_{\text{KL}}}{\partial \sigma^2}(\hat{\mathbf{R}}, \mathbf{R}) &= \text{Tr} \left(\frac{\partial \mathbf{R}^{-1}}{\partial \sigma^2} \hat{\mathbf{R}} \right) - \frac{\partial \log \text{Det}(\mathbf{R}^{-1}\hat{\mathbf{R}})}{\partial \sigma^2} \quad (92) \\ &= + \text{Tr} \left(\frac{\partial \mathbf{R}^{-1}}{\partial \sigma^2} \hat{\mathbf{R}} \right) - \text{Tr} \left\{ (\mathbf{R}^{-1}\hat{\mathbf{R}})^{-1} \frac{\partial (\mathbf{R}^{-1}\hat{\mathbf{R}})}{\partial \sigma^2} \right\} \\ &= + \text{Tr} \left(\frac{\partial \mathbf{R}^{-1}}{\partial \sigma^2} \hat{\mathbf{R}} \right) - \text{Tr} \left\{ (\hat{\mathbf{R}}^{-1}\mathbf{R}) \frac{\partial \mathbf{R}^{-1}}{\partial \sigma^2} \hat{\mathbf{R}} \right\} \\ &= + \text{Tr} \left\{ (\mathbf{I} - \hat{\mathbf{R}}^{-1}\mathbf{R}) \frac{\partial \mathbf{R}^{-1}}{\partial \sigma^2} \hat{\mathbf{R}} \right\} \\ &= - \text{Tr} \left\{ (\mathbf{I} - \hat{\mathbf{R}}^{-1}\mathbf{R}) \mathbf{R}^{-1} \frac{\partial \mathbf{R}}{\partial \sigma^2} \mathbf{R}^{-1} \hat{\mathbf{R}} \right\} \\ &= - \text{Tr} \left\{ (\mathbf{I} - \hat{\mathbf{R}}^{-1}\mathbf{R}) \mathbf{R}^{-1} \mathbf{a}_\theta \mathbf{a}_\theta^H \mathbf{R}^{-1} \hat{\mathbf{R}} \right\}. \end{aligned}$$

Rearranging the terms in the trace, we immediately get

$$\frac{\partial d_{\text{KL}}}{\partial \sigma^2}(\hat{\mathbf{R}}, \mathbf{R}) = -\mathbf{a}_\theta^H \mathbf{R}^{-1} \hat{\mathbf{R}} (\mathbf{I} - \hat{\mathbf{R}}^{-1}\mathbf{R}) \mathbf{R}^{-1} \mathbf{a}_\theta \quad (93)$$

$$\begin{aligned} &= -(\mathbf{a}_\theta^H \mathbf{R}^{-1} \hat{\mathbf{R}} \mathbf{R}^{-1} \mathbf{a}_\theta - \mathbf{a}_\theta^H \mathbf{R}^{-1} \mathbf{a}_\theta) \\ &= -\frac{1}{(\sigma^2 + 1)^2} \mathbf{a}_\theta^H \hat{\mathbf{R}} \mathbf{a}_\theta + \frac{1}{\sigma^2 + 1}. \quad (94) \end{aligned}$$

where the last equality results from the first aforementioned identity. Matching to zero, we get

$$\sigma^2 = \mathbf{a}_\theta^H \hat{\mathbf{R}} \mathbf{a}_\theta - 1, \quad (95)$$

which achieves the proof of (29).

The power spectrum (30) consists in minimizing w.r.t. σ^2 the KL divergence between \mathbf{R} and $\hat{\mathbf{R}}$ defined by

$$d_{\text{KL}}(\mathbf{R}, \hat{\mathbf{R}}) \triangleq \text{Tr} \left(\hat{\mathbf{R}}^{-1}\mathbf{R} - \mathbf{I} \right) - \log \text{Det}(\hat{\mathbf{R}}^{-1}\mathbf{R}). \quad (96)$$

The value of σ^2 that minimizes the latter expression is obtained by matching to 0 the derivative w.r.t. σ^2 . We have

$$\begin{aligned} \frac{\partial d_{\text{KL}}}{\partial \sigma^2}(\mathbf{R}, \hat{\mathbf{R}}) &= \text{Tr} \left(\hat{\mathbf{R}}^{-1} \frac{\partial \mathbf{R}}{\partial \sigma^2} \right) - \frac{\partial \log \text{Det}(\hat{\mathbf{R}}^{-1}\mathbf{R})}{\partial \sigma^2} \quad (97) \\ &= + \text{Tr} \left(\hat{\mathbf{R}}^{-1} \frac{\partial \mathbf{R}}{\partial \sigma^2} \right) - \text{Tr} \left\{ (\hat{\mathbf{R}}^{-1}\mathbf{R})^{-1} \frac{\partial (\hat{\mathbf{R}}^{-1}\mathbf{R})}{\partial \sigma^2} \right\} \\ &= + \text{Tr} \left(\hat{\mathbf{R}}^{-1} \frac{\partial \mathbf{R}}{\partial \sigma^2} \right) - \text{Tr} \left\{ (\mathbf{R}^{-1}\hat{\mathbf{R}}) \hat{\mathbf{R}}^{-1} \frac{\partial \mathbf{R}}{\partial \sigma^2} \right\} \\ &= \text{Tr} \left\{ (\mathbf{I} - \mathbf{R}^{-1}\hat{\mathbf{R}}) \hat{\mathbf{R}}^{-1} \frac{\partial \mathbf{R}}{\partial \sigma^2} \right\} \\ &= \text{Tr} \left\{ (\mathbf{I} - \mathbf{R}^{-1}\hat{\mathbf{R}}) \hat{\mathbf{R}}^{-1} \mathbf{a}_\theta \mathbf{a}_\theta^H \right\}. \quad (98) \end{aligned}$$

Rearranging the terms in the trace, we immediately get

$$\begin{aligned} \frac{\partial d_{\text{KL}}}{\partial \sigma^2}(\mathbf{R}, \hat{\mathbf{R}}) &= \mathbf{a}_\theta^H (\mathbf{I} - \mathbf{R}^{-1}\hat{\mathbf{R}}) \hat{\mathbf{R}}^{-1} \mathbf{a}_\theta \\ &= \mathbf{a}_\theta^H \hat{\mathbf{R}}^{-1} \mathbf{a}_\theta - \mathbf{a}_\theta^H \mathbf{R}^{-1} \mathbf{a}_\theta \\ &= \mathbf{a}_\theta^H \hat{\mathbf{R}}^{-1} \mathbf{a}_\theta - \frac{1}{\sigma^2 + 1}, \quad (99) \end{aligned}$$

where the last equality results from the first aforementioned identity. Matching to zero, we get

$$\sigma^2 = \frac{1}{\mathbf{a}_\theta^H \hat{\mathbf{R}}^{-1} \mathbf{a}_\theta} - 1, \quad (100)$$

which achieves the proof of (30).

APPENDIX VII
ANALYSIS OF THE LOG-DETERMINANT BEAMFORMER

The Log-Determinant (LD) power spectrum $P_{\text{LD}}(\theta)$ defined in (32) consists in minimizing w.r.t. σ^2 the LD distance between $\hat{\mathbf{R}}$ and \mathbf{R} defined by

$$d_{\text{LD}}^2(\hat{\mathbf{R}}, \mathbf{R}) \triangleq \log \left(\text{Det} \left\{ \frac{\hat{\mathbf{R}} + \mathbf{R}}{2} \right\} \right) - \frac{\log \left(\text{Det} \{ \hat{\mathbf{R}} \mathbf{R} \} \right)}{2}. \quad (101)$$

The value of σ^2 that minimizes $d_{\text{LD}}^2(\hat{\mathbf{R}}, \mathbf{R})$ is obtained by matching to 0 the derivative w.r.t. σ^2 . We immediately get

$$\frac{\partial}{\partial \sigma^2} \log \left(\text{Det} \left\{ \frac{\hat{\mathbf{R}} + \mathbf{R}}{2} \right\} \right) - \frac{1}{2} \frac{\partial}{\partial \sigma^2} \log \left(\text{Det} \{ \hat{\mathbf{R}} \mathbf{R} \} \right) = 0. \quad (102)$$

Note that the log-determinant derivative satisfies the identity $\frac{\partial}{\partial \sigma^2} \log \left(\text{Det} \{ \mathbf{M} \} \right) = \text{Tr} \left\{ \mathbf{M}^{-1} \frac{\partial \mathbf{M}}{\partial \sigma^2} \right\}$. Therefore

$$\begin{cases} \frac{\partial}{\partial \sigma^2} \log \left(\text{Det} \left\{ \frac{\hat{\mathbf{R}} + \mathbf{R}}{2} \right\} \right) = \text{Tr} \left\{ \left(\frac{\hat{\mathbf{R}} + \mathbf{R}}{2} \right)^{-1} \frac{\partial (\hat{\mathbf{R}} + \mathbf{R})}{\partial \sigma^2} \right\} \\ \frac{\partial}{\partial \sigma^2} \log \left(\text{Det} \{ \hat{\mathbf{R}} \mathbf{R} \} \right) = \text{Tr} \left\{ (\hat{\mathbf{R}} \mathbf{R})^{-1} \hat{\mathbf{R}} \frac{\partial (\mathbf{R})}{\partial \sigma^2} \right\} \end{cases} \quad (103)$$

Since the derivative of \mathbf{R} w.r.t. σ^2 is $\mathbf{a}_\theta \mathbf{a}_\theta^H$, we get after few manipulations

$$\begin{cases} \frac{\partial}{\partial \sigma^2} \log \left(\text{Det} \left\{ \frac{\hat{\mathbf{R}} + \mathbf{R}}{2} \right\} \right) = \mathbf{a}_\theta^H \left(\frac{\hat{\mathbf{R}} + \mathbf{R}}{2} \right)^{-1} \mathbf{a}_\theta \\ \frac{\partial}{\partial \sigma^2} \log \left(\text{Det} \{ \hat{\mathbf{R}} \mathbf{R} \} \right) = \mathbf{a}_\theta^H \hat{\mathbf{R}}^{-1} \mathbf{a}_\theta \end{cases} \quad (104)$$

Then, equation (102) yields

$$\mathbf{a}_\theta^H (\hat{\mathbf{R}} + \mathbf{R})^{-1} \mathbf{a}_\theta - \frac{1}{2} \mathbf{a}_\theta^H \mathbf{R}^{-1} \mathbf{a}_\theta = 0. \quad (105)$$

Inserting the expression for \mathbf{R} and \mathbf{R}^{-1} , the latter equation reduces to

$$\mathbf{a}_\theta^H (\hat{\mathbf{R}} + \sigma^2 \mathbf{a}_\theta \mathbf{a}_\theta^H + \mathbf{I})^{-1} \mathbf{a}_\theta = \frac{1}{2} \frac{1}{\sigma^2 + 1}. \quad (106)$$

Invoking the Sherman-Morrison identity, we get after few manipulations,

$$\mathbf{a}_\theta^H (\hat{\mathbf{R}} + \mathbf{I})^{-1} \mathbf{a}_\theta - \frac{\sigma^2 (\mathbf{a}_\theta^H (\hat{\mathbf{R}} + \mathbf{I})^{-1} \mathbf{a}_\theta)^2}{1 + \sigma^2 \mathbf{a}_\theta^H (\hat{\mathbf{R}} + \mathbf{I})^{-1} \mathbf{a}_\theta} = \frac{1}{2} \frac{1}{\sigma^2 + 1}. \quad (107)$$

Simplifying the left-hand terms yields

$$\frac{\mathbf{a}_\theta^H (\hat{\mathbf{R}} + \mathbf{I})^{-1} \mathbf{a}_\theta}{1 + \sigma^2 \mathbf{a}_\theta^H (\hat{\mathbf{R}} + \mathbf{I})^{-1} \mathbf{a}_\theta} = \frac{1}{2} \frac{1}{\sigma^2 + 1}. \quad (108)$$

Rearranging the latter equation and setting $P_{\text{LD}}(\theta) = \sigma^2$, we get the Log-Determinant beamformer

$$P_{\text{LD}}(\theta) = \frac{1}{\mathbf{a}_\theta^H (\hat{\mathbf{R}} + \mathbf{I})^{-1} \mathbf{a}_\theta} - 2. \quad (109)$$

It achieves the proof of (32).

We now check that the Log-Determinant metric is indeed invariant to matrix inversion. To that end, we evaluate:

$$d_{\text{LD}}^2 (\hat{\mathbf{R}}^{-1}, \mathbf{R}^{-1}) = \log \left(\text{Det} \left\{ \frac{\hat{\mathbf{R}}^{-1} + \mathbf{R}^{-1}}{2} \right\} \right) - \frac{\log \left(\text{Det} \left\{ \frac{\hat{\mathbf{R}}^{-1} \mathbf{R}^{-1}}{2} \right\} \right)}{2} = \quad (110)$$

$$\log \left(\text{Det} \left\{ \frac{\hat{\mathbf{R}}^{-1} (\hat{\mathbf{R}} + \mathbf{R}) \mathbf{R}^{-1}}{2} \right\} \right) + \frac{\log \left(\text{Det} \left\{ \frac{\hat{\mathbf{R}} \mathbf{R}}{2} \right\} \right)}{2} = \quad (111)$$

$$\log \left(\text{Det} \left\{ \frac{\hat{\mathbf{R}} + \mathbf{R}}{2} \right\} \text{Det} \left\{ \hat{\mathbf{R}}^{-1} \mathbf{R}^{-1} \right\} \right) + \frac{\log \left(\text{Det} \left\{ \frac{\hat{\mathbf{R}} \mathbf{R}}{2} \right\} \right)}{2} = \quad (112)$$

$$\log \left(\text{Det} \left\{ \frac{\hat{\mathbf{R}} + \mathbf{R}}{2} \right\} / \text{Det} \left\{ \frac{\hat{\mathbf{R}} \mathbf{R}}{2} \right\} \right) + \frac{\log \left(\text{Det} \left\{ \frac{\hat{\mathbf{R}} \mathbf{R}}{2} \right\} \right)}{2} = \quad (113)$$

$$\log \left(\text{Det} \left\{ \frac{\hat{\mathbf{R}} + \mathbf{R}}{2} \right\} \right) - \log \left(\text{Det} \left\{ \frac{\hat{\mathbf{R}} \mathbf{R}}{2} \right\} \right) + \frac{\log \left(\text{Det} \left\{ \frac{\hat{\mathbf{R}} \mathbf{R}}{2} \right\} \right)}{2} \quad (114)$$

$$= d_{\text{LD}}^2 (\hat{\mathbf{R}}, \mathbf{R}). \quad (115)$$

This results proves that the Log-Determinant metric is invariant to inversion.